Development 139, 4439-4448 (2012) doi:10.1242/dev.081745

Autotaxin/Lpar3 signaling regulates Kupffer's vesicle formation and left-right asymmetry in zebrafish

Shih-Lei Lai[1], Wan-Ling Yao[1], Ku-Chi Tsao[1], Anna J. S. Houben[2], Harald M. H. G. Albers[2], Huib Ovaa[2], Wouter H. Moolenaar[2] and Shyh-Jye Lee[1,3,4,5,6,*]

SUMMARY

Left-right (L-R) patterning is essential for proper organ morphogenesis and function. Calcium fluxes in dorsal forerunner cells (DFCs) are known to regulate the formation of Kupffer's vesicle (KV), a central organ for establishing L-R asymmetry in zebrafish. Here, we identify the lipid mediator lysophosphatidic acid (LPA) as a regulator of L-R asymmetry in zebrafish embryos. LPA is produced by Autotaxin (Atx), a secreted lysophospholipase D, and triggers various cellular responses through activation of specific G protein-coupled receptors (Lpar1-6). Knockdown of Atx or LPA receptor 3 (Lpar3) by morpholino oligonucleotides perturbed asymmetric gene expression in lateral plate mesoderm and disrupted organ L-R asymmetries, whereas overexpression of *lpar3* partially rescued those defects in both *atx* and *lpar3* morphants. Similar defects were observed in embryos treated with the Atx inhibitor HA130 and the Lpar1-3 inhibitor Ki16425. Knockdown of either Atx or Lpar3 impaired calcium fluxes in DFCs during mid-epiboly stage and compromised DFC cohesive migration, KV formation and ciliogenesis. Application of LPA to DFCs rescued the calcium signal and laterality defects in *atx* morphants. This LPA-dependent L-R asymmetry is mediated via Wnt signaling, as shown by the accumulation of β-catenin in nuclei at the dorsal side of both *atx* and *lpar3* morphants. Our results suggest a major role for the Atx/Lpar3 signaling axis in regulating KV formation, ciliogenesis and L-R asymmetry via a Wnt-dependent pathway.

KEY WORDS: Autotaxin, Lysophosphatidic acid, Calcium, Left-right asymmetry, Zebrafish

INTRODUCTION

Left-right (L-R) patterning is a fundamental process in vertebrate embryogenesis. Establishment of L-R asymmetry in vertebrates has been studied extensively and two embryonic structures are essential for proper L-R patterning: the node (or Kupffer's vesicle, KV, in zebrafish) and the midline, mainly consisting of the floor plate and notochord (Capdevila et al., 2000; Raya and Izpisúa Belmonte, 2006). An intact midline serves as a barrier and, along with *lefty1* expression at the midline, prevents the left-side signals from leaking to the right side (Spéder et al., 2007). KV is a ciliated organ originating from dorsal forerunner cells (DFCs), a group of non-involuting cells at the leading edge of the embryonic shield (dorsal organizer) (Essner et al., 2005; Hirokawa et al., 2006; Raya and Izpisúa Belmonte, 2008). The architecture of KV cells and asymmetric KV cilia along the anterior-posterior (AP) axis generate a counter-clockwise nodal flow. The nodal flow then leads to the asymmetrical expression of early laterality genes, such as nodal-related *southpaw* (*spaw*) and its downstream targets *pitx2* and *lefty*, in the left lateral plate mesoderm (LPM) (Yost, 1999; Capdevila et al., 2000; Long et al., 2003; Hirokawa et al., 2006; Raya and Izpisúa Belmonte, 2006; Spéder et al., 2007; Wang et al., 2011). During the mid-epiboly stage, elevated calcium levels at the shield/DFCs region are essential for the cohesive migration of DFCs to form KV in the tail bud during later stages. Loss of calcium signaling perturbs KV formation and L-R patterning (Schneider et al., 2008). However, the signal transduction pathway leading to the calcium rise remains unknown.

Lysophosphatidic acid (LPA) is a multifunctional lipid mediator that is produced in many tissues and in blood (Moolenaar et al., 2004). LPA is mainly produced from lysophosphatidylcholine by a secreted lysophospholipase D (lysoPLD), named Autotaxin (Atx; Enpp2 – Zebrafish Information Network), originally identified as an autocrine motility factor for tumor cells (Stracke et al., 1992; for a review, see van Meeteren and Moolenaar, 2007). LPA acts on six cognate G protein-coupled receptors, Lpar1-6, in mammals (Choi et al., 2010; Chun et al., 2010). By coupling to multiple G proteins, LPA receptors convey various downstream signals, including activation of Ras and Rho GTPases, phosphoinositide-3-kinase and phospholipase C and mobilization of calcium (Moolenaar et al., 2004; Choi et al., 2010). These signals are then translated into altered gene transcription (Stortelers et al., 2008) and a wide range of cellular responses, including stimulation of cell proliferation, migration and survival as well as cytoskeletal reorganization and morphological changes (Fukushima et al., 1998; Moolenaar et al., 2004; Choi et al., 2010). In mice, Atx and LPA signaling are critically involved in vascular development (Tanaka et al., 2006; van Meeteren et al., 2006b), nervous system function (Fukushima et al., 2002; Yuan et al., 2003; Matas-Rico et al., 2008), lymphocyte homing (Kanda et al., 2008) and tumor progression (Mills and Moolenaar, 2003; Houben and Moolenaar, 2011). Knockout of the genes encoding the three major and closely related LPA receptors (Lpar1-3) in mice resulted in relatively mild phenotypes (Choi et al., 2008). *Lpar1*$^{-/-}$ mice show perinatal lethality due to defective suckling (Contos et al., 2000). In addition, defects in neural development have also been observed (Matas-Rico et al., 2008). *Lpar2*$^{-/-}$ mice show no obvious abnormalities, whereas *Lpar1*$^{-/-}$/*Lpar2*$^{-/-}$ double-null mutants have an exacerbation of the frontal hematomas present in the *Lpar1*$^{-/-}$ mutants (Contos et al., 2002). *Lpar3*$^{-/-}$ mice are viable and grossly normal, but pregnant

[1]Institute of Zoology, [3]Department of Life Science, [4]Center for Systems Biology, [5]Center for Biotechnology, [6]Research Center for Developmental Biology and Regenerative Medicine, National Taiwan University, 1 Roosevelt Road, Sec. 4, Taipei 10617, Taiwan, Republic of China. [2]Division of Cell Biology, The Netherlands Cancer Institute, 1066 CX Amsterdam, The Netherlands.

*Author for correspondence (jefflee@ntu.edu.tw)

Accepted 4 September 2012

female nulls show delayed implantation, altered embryo spacing and reduced litter size (Ye et al., 2005).

Atx is encoded by *Enpp2*. *Enpp2*$^{-/-}$ knockout mice die at E9.5 with severe vascular defects (Tanaka et al., 2006; van Meeteren et al., 2006b). Similarly, *Lpar4*$^{-/-}$ mice display hemorrhages and/or edema and some embryos die during gestation (Sumida et al., 2010), but the phenotype is much less severe than that of the *Enpp2* knockout. We previously showed that *lpar1* is essential for lymphatic vessel development in zebrafish (Lee et al., 2008). A recent study showed that Atx regulates vascular development via multiple LPA receptors in zebrafish (Yukiura et al., 2011). However, it remains unknown to what extent LPA signaling might affect early embryonic development, including L-R patterning.

In this study, we describe a novel role for Atx and Lpar3 in L-R patterning in zebrafish embryos. We find that Atx is highly expressed in the shield during mid-epiboly, and knockdown of either Atx or Lpar3 abolishes calcium fluxes in DFCs at the same embryonic stage. This, in turn, disrupts later KV formation and ciliogenesis, leading to disrupted asymmetric gene expression and organ morphogenesis. Similar effects on L-R asymmetry were observed in embryos treated with inhibitors and antagonists of Atx and Lpar1-3, respectively, and by knockdown of Atx and Lpar3. Taken together, our results reveal a novel role for Atx/LPA signaling in L-R patterning during early zebrafish development.

MATERIALS AND METHODS

Zebrafish

Wild-type AB zebrafish (*Danio rerio*), *Tg(sox17:dsRed)* and *Tg(sox17:GFP)* fish (obtained from Zebrafish International Resource Center, ZIRC) were maintained at 28.5°C on a 14-hour light/10-hour dark cycle. Embryos collected from natural mating were cultured and staged according to Kimmel et al. (Kimmel et al., 1995).

Embryo microinjections

Antisense morpholinos designed against *atx* (tMO: CTGGTG-GCTCTCTTCCACACTGAAC; sMO: GGAGAATACCTGGGTCGA-GACACCG) and *lpar3* (MO1: TTGGACAAAACCCACTAG-GACAGTG; MO2: TAGCAGATGTTGTGCCTGGCCAT) and a standard control morpholino (MO) with random sequence (Std MO: CCTCTTAC-CTCAGTTACAATTTATA) were custom-synthesized by Gene Tools. Full-length coding sequences of *atx* and *lpar3* with or without 5′UTR MO-binding region were cloned from zebrafish cDNAs into the pCS2+ vector for MO efficiency check, and into pcDNA for ectopic expression. Plasmids for injection were prepared using the QIAGEN Plasmid Midi Kit (QIAGEN, Valencia, CA, USA). Capped mRNAs were transcribed with the mMESSAGE mMACHINE Kit (Invitrogen, Carlsbad, CA, USA). LPA (Sigma, St Louis, MO, USA) was applied as previously described (Liao et al., 2005). All reagents were injected at the one-cell stage, unless stated otherwise. DFC-targeted MO/mRNA delivery was performed by microinjecting materials into the yolk syncytial layer of 512- to 1000-cell-stage embryos, as previously reported (Amack and Yost, 2004).

Whole-mount in situ hybridization

DNA fragments of *atx* and *lpar3* were cloned from zebrafish cDNAs by RT-PCR and subcloned into pGEMT-easy vectors for probe synthesis. *southpaw*, *lefty1*, *lefty2*, *pitx2*, *charon* (*dand5*), *cmlc2* (*myl7*), *ntl*, *lrdr* (*dnah9*) and *sox17* were kindly provided by Sheng-Ping Huang (Academia Sinica, Taiwan); *foxA3* was obtained from Chin-Hwa Hu (National Taiwan Ocean University, Taiwan). Whole-mount in situ hybridization was performed as described (Thisse and Thisse, 2008). Stained embryos were mounted in 1% methylcellulose, observed under a Leica MZ75 stereomicroscope (Leica Microsystems, Wetzlar, Germany) and photographed using a Canon 7D DSLR camera (Canon, Lake Success, NY, USA).

Autotaxin inhibitors, LPAR antagonist and in vitro activity assay

The Autotaxin inhibitors HA51 and HA130 were synthesized as described (Albers et al., 2010). HA51 and HA130 were dissolved in DMSO and diluted to the desired concentration. Human ATX (hATX; ENPP2) and zebrafish Atx (zAtx) were expressed in HEK293T cells for in vitro activity assays. LysoPLD activity of ATX in the medium was measured by the hydrolysis of the fluorescent lysophospholipid substrate FS3 (2.5 μM), as described previously (Ferguson et al., 2006). The LPAR inhibitor Ki16425 was applied as described (Yukiura et al., 2011).

Immunofluorescence, confocal microscopy and western blotting

Whole-mount immunofluorescence staining of KV cilia and atypical protein kinase C (aPKC) was performed as previously described (Essner et al., 2005) using an acetylated tubulin antibody (1:400, Sigma) and an aPKC antibody (1:200, Santa Cruz Biotechnology, Santa Cruz, CA, USA). Secondary antibodies used were: Rhodamine Red-X-AffiniPure goat anti-mouse IgG (1:500, Jackson ImmunoResearch Laboratories, West Grove, PA, USA), goat anti-mouse FITC-conjugated IgG (1:500, Abnova, Taipei, Taiwan) and FITC-conjugated goat anti-rabbit IgG (1:500, Sigma). Tail buds from the stained embryos were manually dissected and mounted in SlowFade (Invitrogen) before KV cilia observation and quantification. Three-dimensional image stacks of cilia in a given KV were captured using a Zeiss LSM 780 laser scanning microscope (Carl Zeiss MicroImaging, Göttingen, Germany), and processed using ImageJ software. Cilia number and volume were also analyzed using ImageJ (Object Counter 3D). Similarly, an Atx antibody (1:250, Abnova) and FITC-conjugated goat anti-rabbit IgG (1:500, Sigma) were used to probe Atx. Stained embryos were treated with SlowFade (Invitrogen) and Rhodamine Phalloidin (1:1000, Invitrogen) before observation. Whole-mount immunofluorescence staining of β-catenin and GFP was carried out using a β-catenin antibody (1:250, Sigma) and a GFP antibody (1:250, GeneTex International Corp., Hsinchu, Taiwan) as described (Essner et al., 2005). Embryos were mounted in SlowFade with DAPI (Invitrogen). Colocalization was analyzed and quantified using ImageJ software. Images were collected using a Leica TCS SP5 confocal microscope system (Leica Microsystems) and an LSM 780 confocal laser-scanning microscope (Carl Zeiss, Oberkochen, Germany). Atx immunostaining was observed under a Leica DM2500 DIC microscope (10× objective; Leica Microsystems) and photographed using a CoolSNAP *fx* CCD camera (Roper Scientific, Evry, France). The Atx antibody was used at 1:400 for western blotting as described (Lai et al., 2005).

Calcium imaging and analysis

Fura-2 dextran (Invitrogen) was co-injected with MOs at the one-cell stage. Morphants were mounted in 1% low-melting agarose and examined for the 340/380 nm intensity ratio using a Leica DM2500 DIC microscope (10× objective; Leica Microsystems). In rescue experiments, LPA was injected (0.25 mM pipette concentration) into the yolk syncytial layer (YSL) or the yolk. Images were taken by a CoolSNAP *fx* CCD camera (Roper Scientific) and subjected to ImageJ software. Quantification was carried out by measuring the 340/380 nm intensity ratio.

Statistical analysis

All experimental values are presented as mean ± standard error and were analyzed by one-way ANOVA. Groups denoted with different lettering refer to statistical significance ($P<0.05$).

RESULTS

Loss of Atx and/or Lpar3 results in organ laterality defects

We cloned zebrafish *lpar3* (NCBI number XM689898) by RT-PCR and obtained its 5′ and 3′ sequences by rapid amplification of cDNA ends (RACE; sequence submitted to GeneBank, number JQ400025). Sequence analysis revealed that Lpar3 contains seven transmembrane domains (supplementary material Fig. S1A) and is 62% identical to its human and mouse homologs. Phylogenetic tree analysis grouped zebrafish Lpar3 with human and mouse Lpar3

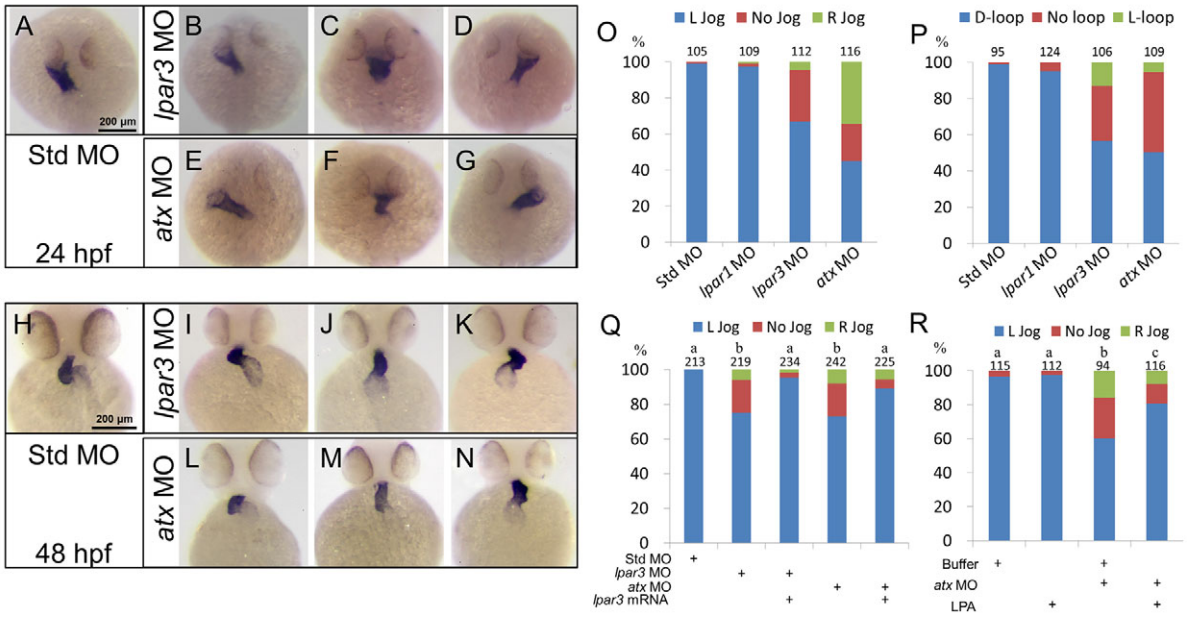

Fig. 1. The Atx-Lpar3 axis mediates cardiac laterality. (**A-P**) Zebrafish embryos injected with 5 ng of different MOs were examined for cardiac jogging at 24 hpf (A-G) or cardiac looping at 48 hpf (H-N) by WISH against *cmlc2*. Representative heart phenotypes are shown for embryos injected with MOs as follows: (A,B,E) left-jogging, (C,F) no-jogging, (D,G) right-jogging, (H,I,L) D-looping, (J,M) no-loop and (K,N) L-looping hearts. In three trials, the percentages of embryos with different heart jogging (O, 24 hpf) and looping phenotypes (P, 48 hpf) are presented. (**Q**) Embryos were injected with 2.5 ng Std MO, *lpar3* MO or *atx* MO with or without 100 pg *lpar3* mRNA. The percentages of embryos with different heart jogging phenotypes are shown (n=3). (**R**) Cardiac jogging of wild-type embryos and *atx* morphants injected with 2.3 nl of buffer or 0.25 mM LPA (pipette concentration) into the yolk syncytial layer at the 512-cell stage was examined and quantified (n=3). Total number of embryos used in each treatment is shown on top of each column for all bar graphs. a, b, c, groups denoted with different lettering refer to statistical significance (P<0.05).

(supplementary material Fig. S1B). Whole-mount in situ hybridization (WISH) analysis of *lpar3* showed ubiquitous expression patterns during early development up to 24 hours post fertilization (hpf; supplementary material Fig. S1C); *lpar3* mRNA was present at all developmental stages as shown by RT-PCR analysis (supplementary material Fig. S1D), suggesting an important role of *lpar3* during early embryogenesis in zebrafish. We also cloned the zebrafish *atx* gene (*enpp2*) (Nakanaga et al., 2010) and found that it shows a similar ubiquitous expression pattern as *lpar3* during early embryogenesis (supplementary material Fig. S2A). To investigate the role of Atx and Lpar3 in early embryogenesis, we used antisense morpholino oligonucleotides (MOs) against *lpar3* (Chiang et al., 2011) and *atx*. Knockdown efficiency of the translational blocking MO was verified by western blotting (supplementary material Fig. S2B). MO-injected embryos will be referred to as morphants hereafter. *lpar3* morphants were grossly normal with a mild developmental delay at 24 hpf (supplementary material Fig. S3A). However, at 48 hpf, cardiac edema and blood pooling appeared at the ventral site of the yolk sphere of *lpar3* morphants (supplementary material Fig. S3B), unlike embryos injected with a control MO (Std MO). *atx* morphants exhibited similar but more severe cardiac defects (supplementary material Fig. S3A,B). We stained erythrocytes with o-dianisidine in both *atx* and *lpar3* morphants (supplementary material Fig. S3C). Erythrocytes in normal embryos were visible in the peri-cardiac cavity and major blood vessels at 72 hpf (supplementary material Fig. S3C, top). By contrast, *atx* and *lpar3* morphants showed blood cell pooling as evidenced by the expansion of erythrocyte staining to the ventral side of the yolk sphere (supplementary material Fig. S3C, middle). The morphants showed up to 30% less erythrocytes and severe hemorrhage in the brain and eyes (supplementary material Fig. S3C, bottom). The alterations in erythrocyte staining were MO dosage dependent. Embryos were injected with various amounts of Std MO, *lpar1* splicing blocking MO (Lee et al., 2008), *lpar3* MO and *atx* tMO, and the blood pooling defects were quantified (supplementary material Fig. S3D). Both *atx* and *lpar3* MOs showed graded MO dosage responses, whereas hardly any effect was observed in *lpar1* MO- or Std MO-injected embryos. A synergistic effect of *atx* and *lpar3* MOs (at a threshold dosage of 1.25 ng per embryo) was also observed (supplementary material Fig. S3E).

The phenotypes of *lpar3* and *atx* morphants suggest a defect in cardiovascular development. We examined cardiac development by WISH against *cardiac myosin light chain 2* (*cmlc2*). At 24 hpf, untreated control and *lpar1* MO-injected embryos had a left jogging heart, as did most of the Std MO-treated embryos (Fig. 1A; data not shown). By contrast, no jogging, left jogging or right jogging hearts appeared in *lpar3* (Fig. 1B-D) or *atx* (Fig. 1E-G) morphants (Fig. 1B-G,O). At 48 hpf, most of the Std MO or *lpar1*-injected embryos showed a heart tube looping to the right (D-looping) as observed in untreated embryos (Fig. 1H). By contrast, *lpar3* (Fig. 1I-K) and *atx* (Fig. 1L-N) morphants showed cardiac looping laterality defects (Fig. 1I-N,P). To confirm that the *lpar3* MO-induced laterality defects are due to loss of Lpar3, we performed *lpar3* mRNA rescue experiments using *lpar3* mRNA without its 5′ untranslated region. Injection of 100 pg *lpar3* mRNA did not induce a notable phenotype by itself; however, co-injection with *lpar3* MO led to a significant increase in the percentage of normal cardiac jogging (L jogging heart) from 75% to 96%. Moreover, the percentage of normal cardiac jogging in *atx*

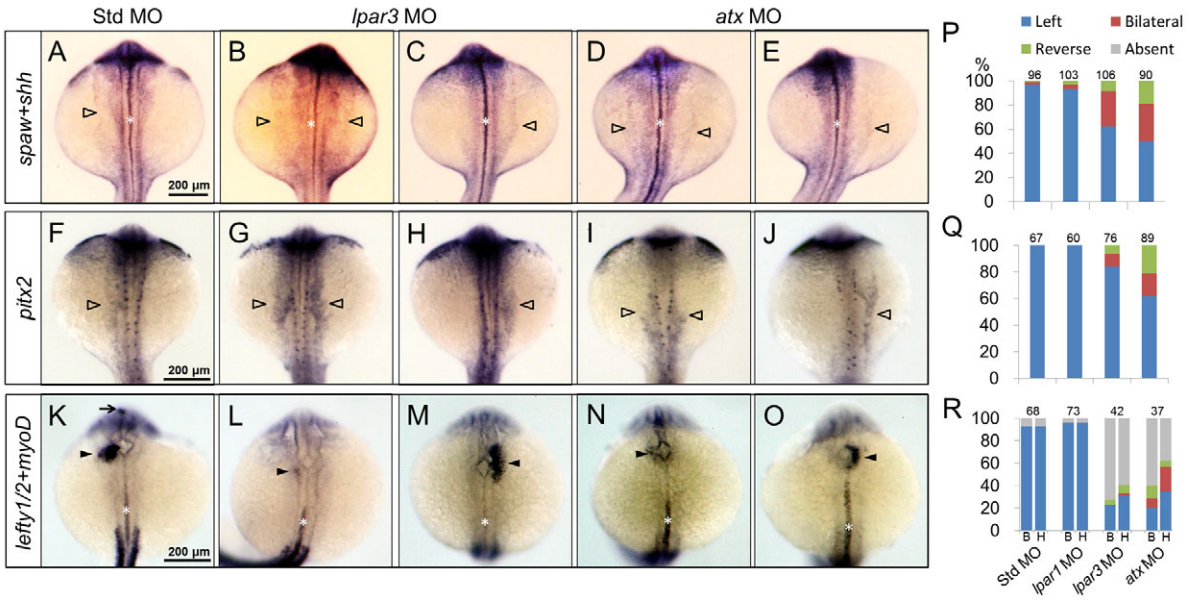

Fig. 2. Asymmetric gene expression is disturbed in *lpar3* and *atx* morphants. (**A-O**) WISH of asymmetry genes *spaw* (A-E), *pitx2* (F-J) and *lefty1* and *lefty2* (K-O) in zebrafish embryos injected with designated MOs are shown. Open arrowheads, lateral plate mesoderm; arrow, diencephalon; solid arrowheads, heart precursor. (**P-R**) Asymmetry genes *spaw* (P), *pitx2* (Q) and *leftys* (R) were quantified in MO-injected embryos. For each treatment, embryos from two independent batches were analyzed. Gene expression in diencephalon (labeled B) and heart precursor (labeled H) were analyzed separately in R.

morphants was partially rescued (from 73% to 89%) by *lpar3* mRNA co-injection (Fig. 1Q). Amack and Yost (Amack and Yost, 2004) showed that microinjecting materials into the yolk syncytial layer (YSL) of 512-cell stage embryos, the injected reagents can be localized to DFCs. Using the same method, we microinjected LPA into the DFCs of *atx* morphants to examine whether the defects were due to the specific loss of LPA in DFCs. LPA by itself had no effect on cardiac jogging in control embryos. By contrast, it significantly increased the percentage of normal L jogging hearts from 60% to 81% (Fig. 1R). Based on these results, we conclude that the Atx/Lpar3 signaling axis is necessary for regulating cardiac laterality.

Defects in heart laterality are often accompanied by impaired gut laterality (Hamada et al., 2002; Raya and Izpisúa Belmonte, 2006). We therefore examined gut looping by WISH against *foxA3*, a marker of the digestive system. Std MO-injected embryos and *lpar1* morphants showed a normal left-looped gut, whereas the *atx* morphants contained gut also in the midline and right side (supplementary material Fig. S4). However, *lpar3* morphants showed only very little midline and reverse gut looping patterns (supplementary material Fig. S4B). This suggests that heart and gut laterality is uncoupled in the *lpar3* morphants.

Atx/Lpar3 signaling regulates asymmetric gene expression

Organ laterality is regulated by asymmetric L-R gene expression (Hirokawa et al., 2006). We analyzed the expression of the nodal-related gene *southpaw* (*spaw*) and its downstream asymmetric genes *lefty1*, *lefty2* and *pitx2*, which form an evolutionarily conserved genetic module in vertebrate L-R patterning (Hamada et al., 2002). At the 21-somite stage, *spaw* (Fig. 2A-E) and *pitx2* (Fig. 2F-J) were both expressed in the left lateral plate mesoderm (LPM) in Std MO-injected embryos and *lpar1* morphants (data not shown), whereas bilateral (Fig. 2B,D,G,I) or reversed expression (Fig. 2C,E,H,J) of both genes appeared in *atx* and *lpar3* morphants (Fig. 2P,Q). Furthermore, expression domains of *lefty1* (left diencephalon) and *lefty2* (left heart primordium) were normal in control embryos and *lpar1* morphants; however, they were largely abolished or reversed in the *atx* and *lpar3* morphants (Fig. 2K-O,R). The intact dorsal midline serves as a barrier to prevent diffusion of asymmetric signals between the L-R sides (Hamada et al., 2002). We examined the integrity of the midline structure by WISH against *sonic hedgehog* (*shh*) and *no tail* (*ntl*). Control, *atx* and *lpar3* morphants showed continuous and straight *shh*, *ntl* and *lefty1* expression at the midline, even in those morphants with bilateral or reversed *spaw* expression (Fig. 2A-E; supplementary material Fig. S6). It thus appears that *atx* and *lpar3* are required for establishing asymmetric gene expression.

Atx and Lpar3 mediate Kupffer's vesicle formation and ciliogenesis

Organ laterality in zebrafish is established by Kupffer's vesicle (KV), an embryonic organ equivalent to the mammalian node. Deformation of KV and/or malfunction of KV cilia can affect organ laterality (Essner et al., 2005; Oishi et al., 2006). Sox17 is expressed in DFC/KV (Kikuchi et al., 2001; Aamar and Dawid, 2010). To examine the effect of Atx and Lpar3 on DFC/KV development, we used two DFC/KV reporter lines, *Tg(sox17:dsRED)* and *Tg(sox17:GFP)*, which express DsRED and GFP, respectively. At the 6-10 somite stage, control *Tg(sox17:dsRED)* embryos showed a normal button-like KV at the terminus of the notochord under bright-field microscopy (Fig. 3A). By contrast, *lpar3* and *atx* morphants both displayed deformed or reduced KVs (Fig. 3B-E). Under dark-field microscopy, KV cells showed a DsRED-labeled fluorescent ring structure (Fig. 3F). Some of the KV cells were dispersed, and the KV ring was disorganized or smaller (Fig. 3G-J). We also used *Tg(sox17:GFP)* embryos to investigate the KV defects in further detail. We found

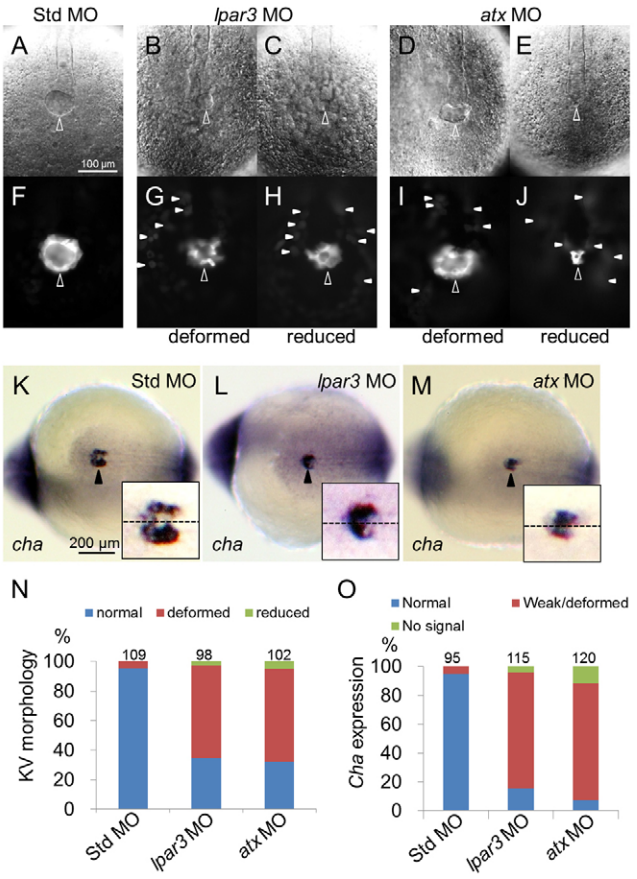

Fig. 3. Kupffer's vesicle formation is disturbed in both *lpar3* and *atx* morphants. (**A-J**,**N**) *Tg(sox17:dsRed)* zebrafish embryos were injected with MO and the integrity of KV was examined under differential interference contrast (A-E) or epifluorescence (F-J) microscopy. In contrast to Std control MO-injected embryos (A,F), deformed (B,G,D,I) and/or reduced KVs (C,H,E,J) were observed in both *lpar3* and *atx* morphants (open arrowheads). In addition, dispersed dsRed-positive cells (arrowheads) were also observed around KV in both *lpar3* and *atx* morphants. To quantify KV defects, *Tg(sox17:dsRed)* embryos were used to repeat the above experiments and analyses are shown in N. (**K-M**,**O**) Embryos injected with the indicated MO were subjected to WISH against *charon* (*cha*, ventral view, bottom right). Arrowheads point to KVs. Magnified KV insets are shown at the lower right of each panel; embryo midlines are indicated by dashed lines. WISH against *charon* also revealed similar deformed/reduced pattern in *lpar3* (L) and *atx* (M) morphants compared with Std control MO-injected embryos (K). Quantitative analyses are shown in O.

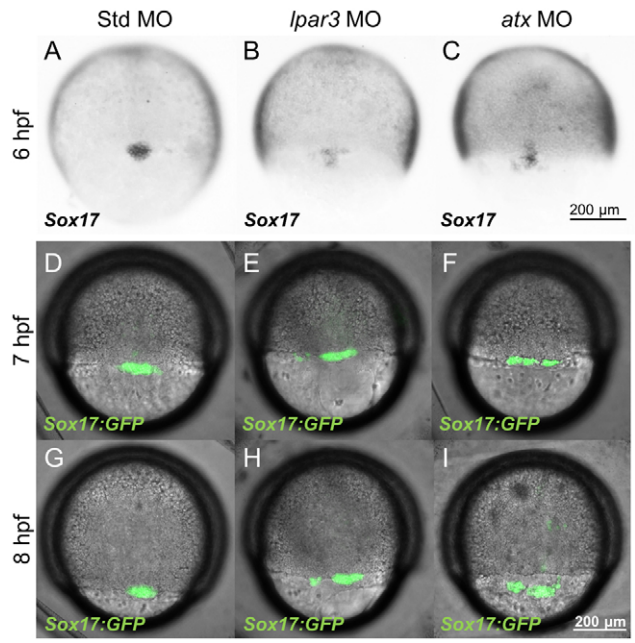

Fig. 4. DFC clustering is disturbed in *lpar3* and *atx* morphants during epiboly. (**A-C**) Zebrafish embryos injected with the indicated MOs were subjected to WISH against *sox17* at 6 hpf. In contrast to the ovoid-shaped DFCs cluster in Std MO-injected embryos (A), dispersed DFC clusters were observed in both *lpar3* (B) and *atx* (C) morphants. (**D-I**) *Tg (sox17:GFP)* embryos were MO injected, cultured to 7 hpf and 8 hpf, and photographed under epifluorescence DIC microscopy. The DIC and epifluorescence images are superimposed and presented. More spread-out and linear-shaped DFCs were observed in both *lpar3* (E,H) and *atx* (F,I) morphants compared with Std MO-injected embryos (D,G).

KVs to be present in all embryos examined. The majority of the defective KVs was deformed, but very few of them were reduced in size (Fig. 3N). KV formation was also examined by WISH against *charon* (*cha*), another KV marker gene (Hashimoto et al., 2004). Unlike the typical *cha* horseshoe expression pattern surrounding the KV in control embryos, with a stronger expression at the right side of the embryo (Fig. 3K), *cha* expression in *lpar3* and *atx* morphants was strongly reduced or missing (Fig. 3L,M,O). Collectively, these results indicate that loss of Atx/Lpar3 signaling leads to aberrant KV formation.

Dispersed DFCs/KV cells resemble the KV phenotype resulting from aberrant DFC clustering and coalescence (Schneider et al., 2008; Matsui et al., 2011). We set out to determine DFC specification and allocation by examining DFC-specific genes. The integrity of the DFC cluster was confirmed by WISH against *sox17* (Fig. 4A-C) in wild-type embryos and by probing GFP in *Tg(sox17:GFP)* embryos (supplementary material Fig. S5). During epiboly progression, DFCs remained as a compact cluster in control embryos (Fig. 4A,D,G), whereas spread-out or fragmented DFC clusters were detected in *atx* and *lpar3* morphants (Fig. 4B,C,E,F,H,J). Despite the distortion of DFC clusters, DFC specification was unaffected in the *atx* and *lpar3* morphants, as shown by DFC-specific expression of sox17 (Fig. 4A-C), *ntl* and *lrdr1* (supplementary material Fig. S6A-I), and DFC migration in transgenic *Tg(sox17:GFP)* embryos (supplementary material Movies 1-6). Next, we examined DFC formation by incubating embryos in media containing 10 μm SYTO-11. SYTO-11 staining showed that *atx* and *lpa3* morphants contained the same number of well-specified DFCs displaying active endocytosis (supplementary material Fig. S6M-O). Defective DFC clustering was again detected in the *atx* and *lpar3* morphants (supplementary material Fig. S6M-O). These data indicate that DFC specification does not depend on Atx/LPA signaling.

To monitor the dynamic changes in DFC clustering and migration, we imaged *Tg(sox17:GFP)* embryos treated with or without MOs against *lpar3* or *atx* (supplementary material Movies 1-6). DFCs in both morphants were dispersed, and formed linear or fragmented cell clusters during migration. They failed to coalesce and to form an intact KV lumen at the tail bud stage (Fig. 4D-I; supplementary material Movies 1-6). This led to a deformed

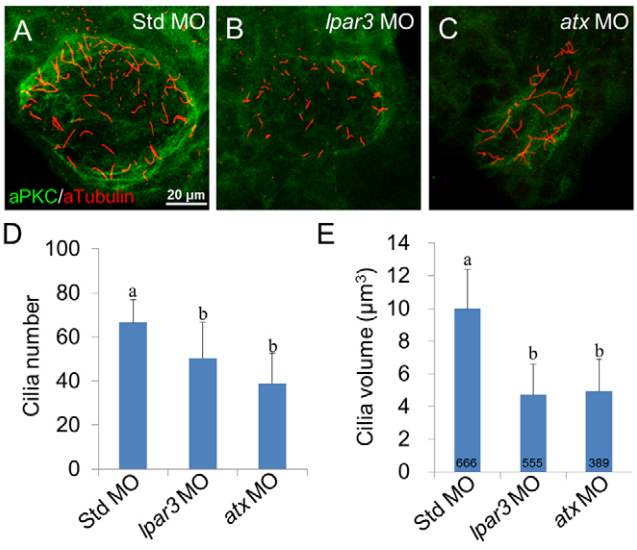

Fig. 5. KV ciliogenesis is disturbed in *lpar3* and *atx* morphants. (**A-C**) Cilia in KV for the indicated treatments were observed by immunofluorescence using anti-acetylated tubulin antibody (red) and counter-stained with aPKC antibody (green) to outline the KV. Representative photographs of Std MO-injected zebrafish embryos (A), *lpar3* (B) and *atx* (C) morphants are presented (anterior side up). (**D**,**E**) Ten embryos were used for each treatment (three independent experiments) to measure cilia number (D) and volume (E). The number of embryos examined is presented in each column. Error bars represent s.e.m. a, b, groups denoted with different lettering refer to statistical significance (P<0.05).

KV, with DFCs failing to coalescence, or to a smaller KV showing dispersed DFCs scattering close to the mature KV (supplementary material Fig. S5 and Movies 4-6). These data strongly suggest that *atx* and *lpa3* are required for DFC clustering and cohesive migration, and for the subsequent coalescence and KV formation.

Primary cilia in KV are known to produce a counter-clockwise flow, which redistributes the early signal molecule Nodal and activated the downstream asymmetry genes *pitx2* and *lefty1/2* (Essner et al., 2005). We examined KV cilia by probing acetylated tubulin and aPKC to outline the KV structure (Fig. 5A-C). Compared with control embryos, *atx* and *lpar3* morphants showed significantly reduced numbers of cilia (Fig. 5D). To examine the cilium length, we scanned serial sections of cilia and measured their volume by 3D-stack analysis (Fig. 5A-C). *atx* and *lpar3* morphants showed a significant reduction in cilia volume (Fig. 5E) and reduced aPKC staining, possibly due to enhanced cell dispersal and/or less DFCs at the KV lumen. From these results, we conclude that the Atx-Lpar3 axis is essential for mediating DFC/KV formation and accompanying ciliogenesis.

The Atx-Lpar3 axis regulates calcium signaling in the shield/DFC region

Calcium signaling in the DFC region during mid-epiboly stages regulates KV formation and organ laterality by antagonizing β-catenin function (Schneider et al., 2008). As LPA is a potent calcium-mobilizing agonist (Moolenaar et al., 2004), we examined whether the laterality defects observed in *atx* and *lpar3* morphants might be due to loss of LPA-induced calcium mobilization. We co-injected fura-2 dextran with the respective MOs and monitored calcium signals in the shield region at the 60% epiboly stage. We observed a local rise in calcium around the shield region with a peak level in DFCs in control embryos, in agreement with previous findings (Schneider et al., 2008) (Fig. 6A). This localized calcium signal was abolished in *lpar3* and *atx* morphants (Fig. 6A,B). Compared with control embryos, the basal calcium levels in the morphants were not altered (ventral counterpart as an example). As shown in Fig. 6B, the dorsal/ventral fura-2 fluorescence ratios in control embryos were significantly higher than those in the *atx* and *lpar3* morphants. Ubiquitous expression of *lpar3* (supplementary material Fig. S1C) and *atx* (supplementary material Fig. S2A) seems difficult to reconcile with the localized regulation of the shield/DFC calcium signal. We therefore examined the localization of Atx and found that it was sporadically distributed in the blastomeres, but with higher levels in the shield region (supplementary material Fig. S7A,C). Atx accumulation was time dependent, as it disappeared before the 80% epiboly stage (supplementary material Fig. S7B). In agreement with the western blotting results (supplementary material Fig. S2B), total Atx was lower in the *atx* morphants, and there was no Atx accumulation in the shield region (supplementary material Fig. S7B,C). In addition, DFC/YSL-targeted delivery of LPA (Fig. 1R) in *atx* morphants restored the calcium signal at the DFC region (Fig. 6C). We double stained nuclei and β-catenin using DAPI (red) and β-catenin antibody (green, with FITC-conjugated goat anti-rabbit secondary antibody), respectively. Pseudocolor image analysis showed that the nuclear localization of β-catenin (supplementary material Fig. S8, white) was significantly higher in the *atx* and *lpar3* morphants, consistent with the notion that loss of LPA-induced DFC calcium signaling leads to Wnt activation. We conclude that Atx/Lpar3 signaling is required for calcium mobilization leading to DFC cohesive migration and coalescence during KV formation in a Wnt-dependent manner.

Atx and Lpar3 function in DFC/KV cells during the mid-epiboly stage to control L-R asymmetry

To investigate the significance of LPA signaling in DFCs, we injected FITC-conjugated *lpar3* MOs into the YSL of 512-cell-stage embryos and detected fluorescent MO in DFCs and the YSL (supplementary material Fig. S9). This allowed us to perform targeted knockdown of Atx and Lpar3 in DFCs. Embryos with targeted gene knockdown in DFCs are referred to as DFC$^{gene\ MO}$ embryos hereafter. Surprisingly, >80% of DFC$^{lpar3\ MO}$ embryos showed normal cardiac jogging unlike those embryos injected MO at the 1-cell stage (Fig. 7A). Instead, the DFC$^{lpar3\ MO}$ embryos exhibited a delay in heart primordium fusion and cardiac bifida in an MO dose-dependent manner (supplementary material Fig. S2E). By contrast, DFC$^{atx\ MO}$ embryos showed impaired laterality, with only a few embryos having heart primordium fusion and bifida defects (Fig. 7A). Co-injection of *lpar3* mRNA significantly rescued the defects in DFC$^{lpar3\ MO}$ embryos (Fig. 7A), but not in DFC$^{atx\ MO}$ embryos. However, it appeared that primordium fusion was reduced by *lpar3* mRNA in DFC$^{atx\ MO}$ embryos. Although the rescue effect was not statistically significant, it is notable and more obvious in morphants injected with 2.5 ng *atx* MO in which reverse jogging (R jog) was significantly reduced (Fig. 7). The disturbed migration and fusion of heart primordium eventually recovered, but these DFC$^{lpar3\ MO}$ embryos still had cardiac looping defects at 48 hpf (Fig. 7B). Similarly, DFC$^{atx\ MO}$ embryos showed fewer laterality defects than did DFC$^{lpar3\ MO}$ embryos in cardiac looping (Fig. 7B).

To determine the active window for LPA during DFC formation, we treated embryos from time points during epiboly

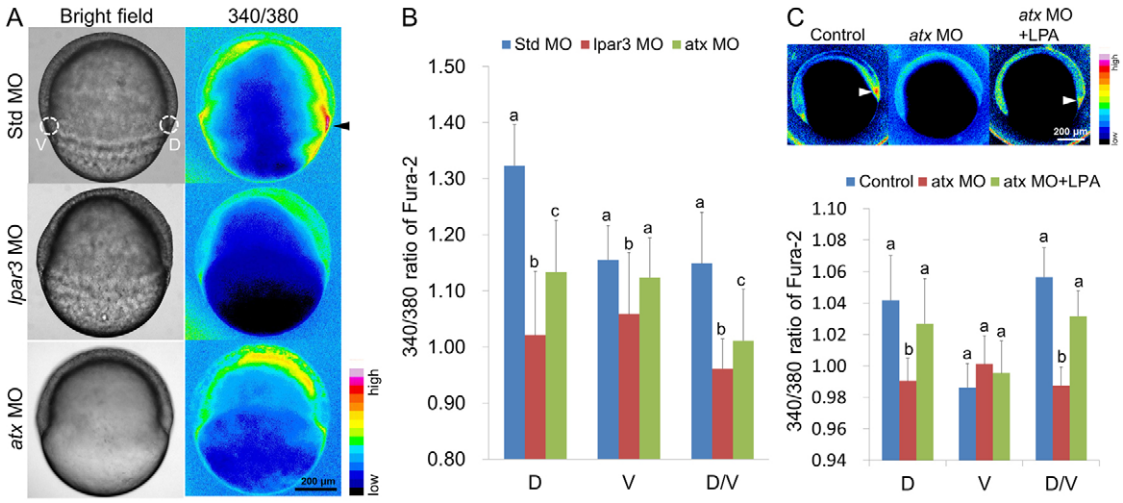

Fig. 6. Calcium rise in the DFCs is abolished in *lpar3* and *atx* morphants. (**A**) Zebrafish embryos were injected with the indicated MOs and fura-2 dextran, incubated to the shield stage and photographed under bright and dark field. The dark-field images were converted to 16-color intensity images (intensity bar is shown in the bottom right corner of A) using Image J software. The shield showed higher calcium levels in control embryos (with peak levels in DFCs; black arrowhead) than those in *lpar3* and *atx* morphants. (**B**) The peak 340/380 nm ratio in the shield/DFCs region (cycles at the dorsal side) and the ventral blastoderm region (cycles at the ventral side) were measured using Image J software (n=10 for each treatment from three independent experiments). The dorsal, ventral and dorsal/ventral 340/380 nm ratios are shown. (**C**) Similar analysis was applied in *atx* morphants with additional DFC-targeting LPA delivery. LPA restores the calcium signal in the shield/DFC region. a, b, c, groups denoted with different lettering refer to statistical significance (P<0.05).

with the Atx inhibitors HA51 and HA130 (Albers et al., 2010). First, we confirmed that zebrafish Atx has lysoPLD activity, using recombinant myc-tagged zAtx expressed in HEK293 cells, and is inhibited by HA51 and HA130, with HA130 being the more potent drug (supplementary material Fig. S2D). Embryos were incubated with HA130 from the 50% epiboly stage until the bud stage (marked as 'E' in supplementary material Fig. S2G). The drug-treated embryos showed prominent dose-dependent defects in cardiac primordium migration at 24 hpf. At 48 hpf, HA130-treated embryos showed defective cardiac looping and blood pooling, as shown by *cmlc2* and o-dianisidine staining. Embryos with a 'no-loop' heart, but not embryos with a reversed L-loop heart, showed more severe expansion of blood cell staining at the ventral side of the yolk sphere (supplementary material Fig. S2F). We also incubated embryos with HA130 from 60% epiboly (marked as 'L' in supplementary material Fig. S2G). Those embryos showed only very mild defects in cardiac primordium migration and jogging. These results indicate that LPA is required between 50 and 60% epiboly, whereas a high calcium flux is required for DFC formation (Schneider et al.,

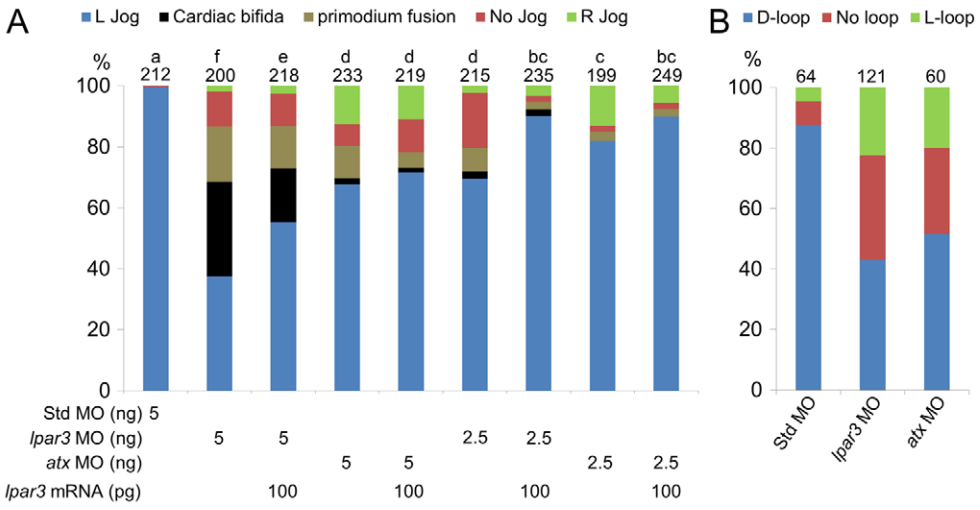

Fig. 7. Targeted knockdown of *lpar3* or *atx* in DFCs causes cardiac bifida in addition to laterality defects. (**A**) Zebrafish embryos at the 512- to 1000-cell stage were injected with 2.5 or 5 ng of the indicated MOs with or without 100 pg of *lpar3* mRNA, as shown at the bottom of each column. Treated embryos were cultured until 26-28 hpf and then subjected to cardiac jogging analysis. The percentages of each phenotype in all treatments are shown in the lower graph. a-f, groups denoted with different lettering refer to statistical significance (P<0.05). (n=3). (**B**) Embryos with the indicated treatments were incubated to 48 hpf and then subjected to cardiac looping analysis.

2008). Next, we tested Ki16425, an antagonist of zebrafish Lpar1-3 (Yukiura et al., 2011). Embryos incubated with Ki16425 from the 50% epiboly to the tail bud stage showed similar effects to observed those with the Atx inhibitor HA130, although somewhat less pronounced (supplementary material Fig. S2H).

DISCUSSION

Establishment of L-R asymmetry is crucial for embryogenesis. Directional fluid flow generated by specialized ciliated epithelial cells is a conserved mechanism underlying L-R asymmetry and occurs at the node in mice and the KV in zebrafish (Nonaka et al., 1998; Essner et al., 2005; Kramer-Zucker et al., 2005). In this study, we discovered a novel mediator of KV formation and L-R asymmetry, namely the Atx-Lpar3 axis. We found that the Atx-Lpar3 axis regulates calcium signaling in the shield/DFCs region to control cohesive migration and clustering of DFCs for proper KV formation and L-R patterning.

LPA signaling has been extensively studied in numerous mammalian cell systems (Moolenaar et al., 2004; Choi et al., 2010). Yet the in vivo functions of LPA signaling are still incompletely understood, despite many studies on Atx and LPA receptor knockout mice (Contos et al., 2000; Contos et al., 2002; Ye et al., 2005; Tanaka et al., 2006; van Meeteren et al., 2006b). Here, we use antisense MOs and Atx inhibitors to dissect the possible roles of LPA signaling during early embryogenesis and found that Atx and Lpar3 regulate L-R patterning. Consistent with previous knockout studies in mice (Tanaka et al., 2006; van Meeteren et al., 2006b; Sumida et al., 2010), we observed defects in cardiovascular development by disturbing Atx/LPA signaling. In addition to vascular defects, the disturbed blood circulation and blood pooling in *atx* and *lpar3* morphants are partly due to heart malformation, resulting from impaired cardiac jogging and looping. This LPA-mediated laterality control is a novel observation, as none of the Atx or LPA receptor knockout studies in mice has hinted at laterality defects during embryogenesis. Atx-deficient mice die at E9.5 with profound vascular defects (van Meeteren et al., 2006a), which might have masked any laterality defect. Furthermore, embryos with L-R defects might be morphologically ‘normal’, thereby escaping detection. Therefore, it would be interesting to re-examine L-R asymmetry phenotypes in Atx knockout embryos. It is of note, however, that the origin, development and ultrastructure of the node in mice versus the KV in zebrafish are different (Supatto and Vermot, 2011). It would therefore be interesting to investigate the possible roles of Atx/LPA signaling in node formation and ciliogenesis during mouse embryogenesis.

Defects in L-R patterning lead to abnormal organ positioning, skeletal malformation, neural tube closure failure and complex congenital heart defects (Bisgrove et al., 2003; Ramsdell, 2005). This is the first study to demonstrate a role of the Atx-Lpar3 axis in regulating L-R asymmetry during embryogenesis. The involvement of G protein-coupled receptors (GPCRs) in L-R asymmetry has been reported previously. In particular, Wnt and Fgf pathways might mediate L-R patterning via GPCRs (Oishi et al., 2006; Hong and Dawid, 2009; Lin and Xu, 2009). Wnt signaling controls KV formation and ciliogenesis via β-catenin-dependent and -independent pathways (Oishi et al., 2006; Lin and Xu, 2009). It has been suggested that LPA might crosstalk with Wnt signaling (Malbon, 2005). Consistent with this, we found a significant increase of nuclear β-catenin in *lpar3* and *atx* morphants, possibly due to reduced calcium signals in the DFC region (Schneider et al., 2008).

Deficiency of both *atx* and *lpar3* altered *spaw* expression at a similar penetrance level, whereas *atx* deficiency showed much higher impact on *pitx2* expression than did *lpar3* deficiency. Also, *lefty2* expression in the left heart primordium and *lefty1* in diencephalon are largely missing in *atx* and *lpar3* morphants. This agrees with the fact that expression of *nodal*, *pitx2* and *lefty2* are not always correlated. *lefty2* expression can be ectopically induced in the absence of *nodal* expression, or it can be abolished in the presence of *nodal* (Chocron et al., 2007; Shu et al., 2007). The expression of *lefty1* and *lefty2* is sometimes abolished in the presence of *spaw* in zebrafish morphants (Schneider et al., 2008; Lin and Xu, 2009; Francescatto et al., 2010; Zhang et al., 2012). The differential expression of *lefty1* in notochord and *lefty1* and *lefty2* in brain and heart has been reported previously (Chocron et al., 2007). Our results further support the uncoupling of different organ laterality.

Embryos defective in L-R asymmetry often show altered visceral laterality (Hamada et al., 2002). The laterality uncoupling between gut and heart that we observed in *lpar3* morphants also occurs in zebrafish embryos overexpressing Wnt3 and Wnt8 (Lin and Xu, 2009), *deltaD* mutants (Lopes et al., 2010) and the *laf/alk8* (*acvr1l*) mutant (Chocron et al., 2007). This suggests that additional LPA receptors and/or other signaling pathways are involved during later organ morphogenesis, or that LPA signaling through Lpar3 is required at a later developmental stage, resembles Bmp signaling in the regulation of L-R asymmetry. Our results, along with previous findings, suggest that complex signaling cross-talk underlies asymmetric gene expression and subsequent control of organ laterality.

Calcium signaling in the DFCs region has been implicated in KV formation (Schneider et al., 2008) and occurs downstream of LPA receptor stimulation through activation of phospholipase C (Moolenaar et al., 2004; Schneider et al., 2008; Choi et al., 2010). We observed localized calcium signals at the shield/DFCs region, which was abolished in embryos lacking *atx* or *lpar3*. Although *atx* mRNA was ubiquitously expressed in early embryos, Atx protein was enriched in the shield region. Thus, part of LPA produced by the shield blastomeres might activate neighboring DFCs in a paracrine fashion. Consistent with this, DFC^{atxMO} embryos showed less severe defects than did $DFC^{lpar3\ MO}$ embryos, whereas Atx knockdown has higher penetrance than *lpar3* knockdown in other loss-of-function experiments. LPA signaling induces a local calcium release in shield/DFCs region, presumably through Lpa3-mediated calcium mobilization.

LPA signaling also leads to activation of Rho family GTPases that regulate cell shape (Moolenaar et al., 2004; Choi et al., 2010). The shape of ciliated KV cells is asymmetric along the AP axis. Anterior KV cells are long and narrow with small apical surfaces, whereas posterior KV cells are short and wide and have a larger apical surface. AP asymmetry of KV cell arrangement thus results in more cilia in the anterior half than the posterior, and produces directional nodal flow to establish L-R asymmetry (Wang et al., 2011). We observed a similar feature, in that KV cells are irregularly shaped and lost their AP morphologies around the KV in *atx* and *lpar3* morphants. As a consequence, asymmetric distribution of cilia number along the AP axis was abolished. It remains possible that LPA signaling is also involved at later steps to establish AP asymmetry of KV cells, for example through activation of Rho GTPases. Although KV formation may not be comparable to node formation in mice, and ciliogenesis defects in *atx* and *lpar3* morphants could be secondary to malformed KV, further studies on ciliogenesis and laterality defects in *Enpp2* and *Lpar* knockout mice are warranted.

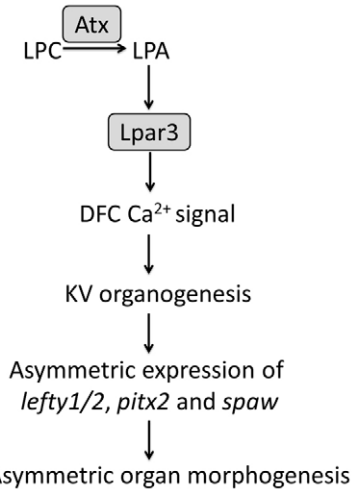

Fig. 8. Atx/Lpar3 signaling in the regulation of L-R asymmetry during zebrafish development. In our model, Atx-produced LPA signals through Lpar3 to induce calcium mobilization in the shield, leading to KV formation from DFCs and to ciliogenesis. Asymmetric gene expression induced by KV subsequently regulates organ laterality and morphogenesis.

Taken together, our results reveal a unique role for Atx and Lpar3 in mediating L-R asymmetry via regulation of calcium signaling in the shield/DFC region, which regulates KV formation and ciliogenesis. As illustrated in Fig. 8, proper KV formation and ciliogenesis then establishes asymmetry in gene expression and organ laterality during zebrafish development.

Acknowledgements
We thank Drs Sheng-Ping Huang, Dr Wen-Pin Wang and Chin-Hwa Hu and Taiwan Zebrafish core facility for providing technical guidance, plasmids and reagents, in particular Dr Sheng-Ping Huang for the help in the gut asymmetric gene expression analysis; Ms Yi-Chun Chuang in Technology Commons in National Taiwan University for excellent technical assistance with confocal microscopy; and Drs Yu-Ting Yan and Chien-Yuan Pan for helpful discussions.

Funding
S.-L.L. was a recipient of postdoctoral fellowships from National Science Council and National Taiwan University. This work was supported by the National Science Council [NSC-98-2311-B-002-006-MY3]; National Taiwan University [NTU CESRP-10R70602A5 and NTU ERP-10R80600 to S.-J.L.]; and the Dutch Cancer Society [W.H.M. and H.O.].

Competing interests statement
The authors declare no competing financial interests.

Supplementary material
Supplementary material available online at
http://dev.biologists.org/lookup/suppl/doi:10.1242/dev.081745/-/DC1

References

Aamar, E. and Dawid, I. B. (2010). Sox17 and chordin are required for formation of Kupffer's vesicle and left-right asymmetry determination in zebrafish. *Dev. Dyn.* **239**, 2980-2988.
Albers, H. M., Dong, A., van Meeteren, L. A., Egan, D. A., Sunkara, M., van Tilburg, E. W., Schuurman, K., van Tellingen, O., Morris, A. J., Smyth, S. S. et al. (2010). Boronic acid-based inhibitor of autotaxin reveals rapid turnover of LPA in the circulation. *Proc. Natl. Acad. Sci. USA* **107**, 7257-7262.
Amack, J. D. and Yost, H. J. (2004). The T box transcription factor no tail in ciliated cells controls zebrafish left-right asymmetry. *Curr. Biol.* **14**, 685-690.
Bisgrove, B. W., Morelli, S. H. and Yost, H. J. (2003). Genetics of human laterality disorders: insights from vertebrate model systems. *Annu. Rev. Genomics Hum. Genet.* **4**, 1-32.
Capdevila, J., Vogan, K. J., Tabin, C. J. and Izpisúa Belmonte, J. C. (2000). Mechanisms of left-right determination in vertebrates. *Cell* **101**, 9-21.
Chiang, C.-L., Chen, S.-S. A., Lee, S. J., Tsao, K.-C., Chu, P.-L., Wen, C.-H., Hwang, S.-M., Yao, C.-L. and Lee, H. (2011). Lysophosphatidic acid induces erythropoiesis through activating lysophosphatidic acid receptor 3. *Stem Cells* **29**, 1763-1773.
Chocron, S., Verhoeven, M. C., Rentzsch, F., Hammerschmidt, M. and Bakkers, J. (2007). Zebrafish Bmp4 regulates left-right asymmetry at two distinct developmental time points. *Dev. Biol.* **305**, 577-588.
Choi, J. W., Lee, C. W. and Chun, J. (2008). Biological roles of lysophospholipid receptors revealed by genetic null mice: an update. *Biochim. Biophys. Acta* **1781**, 531-539.
Choi, J. W., Herr, D. R., Noguchi, K., Yung, Y. C., Lee, C. W., Mutoh, T., Lin, M. E., Teo, S. T., Park, K. E., Mosley, A. N. et al. (2010). LPA receptors: subtypes and biological actions. *Annu. Rev. Pharmacol. Toxicol.* **50**, 157-186.
Chun, J., Hla, T., Lynch, K. R., Spiegel, S. and Moolenaar, W. H. (2010). International Union of Basic and Clinical Pharmacology. LXXVIII. Lysophospholipid receptor nomenclature. *Pharmacol. Rev.* **62**, 579-587.
Contos, J. J., Fukushima, N., Weiner, J. A., Kaushal, D. and Chun, J. (2000). Requirement for the lpA1 lysophosphatidic acid receptor gene in normal suckling behavior. *Proc. Natl. Acad. Sci. USA* **97**, 13384-13389.
Contos, J. J. A., Ishii, I., Fukushima, N., Kingsbury, M. A., Ye, X. Q., Kawamura, S., Brown, J. H. and Chun, J. (2002). Characterization of lpa(2) (Edg4) and lpa(1)/lpa(2) (Edg2/Edg4) lysophosphatidic acid receptor knockout mice: signaling deficits without obvious phenotypic abnormality attributable to lpa(2). *Mol. Cell. Biol.* **22**, 6921-6929.
Essner, J. J., Amack, J. D., Nyholm, M. K., Harris, E. B. and Yost, H. J. (2005). Kupffer's vesicle is a ciliated organ of asymmetry in the zebrafish embryo that initiates left-right development of the brain, heart and gut. *Development* **132**, 1247-1260.
Ferguson, C. G., Bigman, C. S., Richardson, R. D., van Meeteren, L. A., Moolenaar, W. H. and Prestwich, G. D. (2006). Fluorogenic phospholipid substrate to detect lysophospholipase D/autotaxin activity. *Org. Lett.* **8**, 2023-2026.
Francescatto, L., Rothschild, S. C., Myers, A. L. and Tombes, R. M. (2010). The activation of membrane targeted CaMK-II in the zebrafish Kupffer's vesicle is required for left-right asymmetry. *Development* **137**, 2753-2762.
Fukushima, N., Kimura, Y. and Chun, J. (1998). A single receptor encoded by vzg-1/lpA1/edg-2 couples to G proteins and mediates multiple cellular responses to lysophosphatidic acid. *Proc. Natl. Acad. Sci. USA* **95**, 6151-6156.
Fukushima, N., Weiner, J. A., Kaushal, D., Contos, J. J. A., Rehen, S. K., Kingsbury, M. A., Kim, K. Y. and Chun, J. (2002). Lysophosphatidic acid influences the morphology and motility of young, postmitotic cortical neurons. *Mol. Cell. Neurosci.* **20**, 271-282.
Hamada, H., Meno, C., Watanabe, D. and Saijoh, Y. (2002). Establishment of vertebrate left-right asymmetry. *Nat. Rev. Genet.* **3**, 103-113.
Hashimoto, H., Rebagliati, M., Ahmad, N., Muraoka, O., Kurokawa, T., Hibi, M. and Suzuki, T. (2004). The Cerberus/Dan-family protein Charon is a negative regulator of Nodal signaling during left-right patterning in zebrafish. *Development* **131**, 1741-1753.
Hirokawa, N., Tanaka, Y., Okada, Y. and Takeda, S. (2006). Nodal flow and the generation of left-right asymmetry. *Cell* **125**, 33-45.
Hong, S. K. and Dawid, I. B. (2009). FGF-dependent left-right asymmetry patterning in zebrafish is mediated by Ier2 and Fibp1. *Proc. Natl. Acad. Sci. USA* **106**, 2230-2235.
Houben, A. J. and Moolenaar, W. H. (2011). Autotaxin and LPA receptor signaling in cancer. *Cancer Metastasis Rev.* **30**, 557-565.
Kanda, H., Newton, R., Klein, R., Morita, Y., Gunn, M. D. and Rosen, S. D. (2008). Autotaxin, an ectoenzyme that produces lysophosphatidic acid, promotes the entry of lymphocytes into secondary lymphoid organs. *Nat. Immunol.* **9**, 415-423.
Kikuchi, Y., Agathon, A., Alexander, J., Thisse, C., Waldron, S., Yelon, D., Thisse, B. and Stainier, D. Y. R. (2001). casanova encodes a novel Sox-related protein necessary and sufficient for early endoderm formation in zebrafish. *Genes Dev.* **15**, 1493-1505.
Kimmel, C. B., Ballard, W. W., Kimmel, S. R., Ullmann, B. and Schilling, T. F. (1995). Stages of embryonic development of the zebrafish. *Dev. Dyn.* **203**, 253-310.
Kramer-Zucker, A. G., Olale, F., Haycraft, C. J., Yoder, B. K., Schier, A. F. and Drummond, I. A. (2005). Cilia-driven fluid flow in the zebrafish pronephros, brain and Kupffer's vesicle is required for normal organogenesis. *Development* **132**, 1907-1921.
Lai, S. L., Chang, C. N., Wang, P. J. and Lee, S. J. (2005). Rho mediates cytokinesis and epiboly via ROCK in zebrafish. *Mol. Reprod. Dev.* **71**, 186-196.
Lee, S. J., Chan, T. H., Chen, T. C., Liao, B. K., Hwang, P. P. and Lee, H. (2008). LPA1 is essential for lymphatic vessel development in zebrafish. *FASEB J.* **22**, 3706-3715.
Liao, J. J., Huang, Y-T. and Lee, H. (2005). Inhibitory effects of sphingosine 1-phosphate on proliferation of PC-3 human prostate cancer cells. *Zoolog. Studies* **44**, 219-227.
Lin, X. and Xu, X. (2009). Distinct functions of Wnt/beta-catenin signaling in KV development and cardiac asymmetry. *Development* **136**, 207-217.

Long, S., Ahmad, N. and Rebagliati, M. (2003). The zebrafish nodal-related gene southpaw is required for visceral and diencephalic left-right asymmetry. *Development* **130**, 2303-2316.
Lopes, S. S., Lourenço, R., Pacheco, L., Moreno, N., Kreiling, J. and Saúde, L. (2010). Notch signalling regulates left-right asymmetry through ciliary length control. *Development* **137**, 3625-3632.
Malbon, C. C. (2005). Beta-catenin, cancer, and G proteins: not just for frizzleds anymore. *Sci. STKE* **2005**, pe35.
Matas-Rico, E., García-Diaz, B., Llebrez-Zayas, P., López-Barroso, D., Santín, L., Pedraza, C., Smith-Fernández, A., Fernández-Llebrez, P., Tellez, T., Redondo, M. et al. (2008). Deletion of lysophosphatidic acid receptor LPA1 reduces neurogenesis in the mouse dentate gyrus. *Mol. Cell. Neurosci.* **39**, 342-355.
Matsui, T., Thitamadee, S., Murata, T., Kakinuma, H., Nabetani, T., Hirabayashi, Y., Hirate, Y., Okamoto, H. and Bessho, Y. (2011). Canopy1, a positive feedback regulator of FGF signaling, controls progenitor cell clustering during Kupffer's vesicle organogenesis. *Proc. Natl. Acad. Sci. USA* **108**, 9881-9886.
Mills, G. B. and Moolenaar, W. H. (2003). The emerging role of lysophosphatidic acid in cancer. *Nat. Rev. Cancer* **3**, 582-591.
Moolenaar, W. H., van Meeteren, L. A. and Giepmans, B. N. (2004). The ins and outs of lysophosphatidic acid signaling. *Bioessays* **26**, 870-881.
Nakanaga, K., Hama, K. and Aoki, J. (2010). Autotaxin – an LPA producing enzyme with diverse functions. *J. Biochem.* **148**, 13-24.
Nonaka, S., Tanaka, Y., Okada, Y., Takeda, S., Harada, A., Kanai, Y., Kido, M. and Hirokawa, N. (1998). Randomization of left-right asymmetry due to loss of nodal cilia generating leftward flow of extraembryonic fluid in mice lacking KIF3B motor protein. *Cell* **95**, 829-837.
Oishi, I., Kawakami, Y., Raya, A., Callol-Massot, C. and Izpisúa Belmonte, J. C. (2006). Regulation of primary cilia formation and left-right patterning in zebrafish by a noncanonical Wnt signaling mediator, duboraya. *Nat. Genet.* **38**, 1316-1322.
Ramsdell, A. F. (2005). Left-right asymmetry and congenital cardiac defects: getting to the heart of the matter in vertebrate left-right axis determination. *Dev. Biol.* **288**, 1-20.
Raya, A. and Izpisúa Belmonte, J. C. (2006). Left-right asymmetry in the vertebrate embryo: from early information to higher-level integration. *Nat. Rev. Genet.* **7**, 283-293.
Raya, Á. and Izpisúa Belmonte, J. C. (2008). Insights into the establishment of left-right asymmetries in vertebrates. *Birth Defects Res. C: Embryo Today* **84**, 81-94.
Schneider, I., Houston, D. W., Rebagliati, M. R. and Slusarski, D. C. (2008). Calcium fluxes in dorsal forerunner cells antagonize beta-catenin and alter left-right patterning. *Development* **135**, 75-84.
Shu, X., Huang, J., Dong, Y., Choi, J., Langenbacher, A. and Chen, J. N. (2007). Na,K-ATPase alpha2 and Ncx4a regulate zebrafish left-right patterning. *Development* **134**, 1921-1930.
Spéder, P., Petzoldt, A., Suzanne, M. and Noselli, S. (2007). Strategies to establish left/right asymmetry in vertebrates and invertebrates. *Curr. Opin. Genet. Dev.* **17**, 351-358.
Stortelers, C., Kerkhoven, R. and Moolenaar, W. H. (2008). Multiple actions of lysophosphatidic acid on fibroblasts revealed by transcriptional profiling. *BMC Genomics* **9**, 387.
Stracke, M. L., Krutzsch, H. C., Unsworth, E. J., Arestad, A., Cioce, V., Schiffmann, E. and Liotta, L. A. (1992). Identification, purification, and partial sequence analysis of autotaxin, a novel motility-stimulating protein. *J. Biol. Chem.* **267**, 2524-2529.
Sumida, H., Noguchi, K., Kihara, Y., Abe, M., Yanagida, K., Hamano, F., Sato, S., Tamaki, K., Morishita, Y., Kano, M. R. et al. (2010). LPA4 regulates blood and lymphatic vessel formation during mouse embryogenesis. *Blood* **116**, 5060-5070.
Supatto, W. and Vermot, J. (2011). From cilia hydrodynamics to zebrafish embryonic development. *Curr. Top. Dev. Biol.* **95**, 33-66.
Tanaka, M., Okudaira, S., Kishi, Y., Ohkawa, R., Iseki, S., Ota, M., Noji, S., Yatomi, Y., Aoki, J. and Arai, H. (2006). Autotaxin stabilizes blood vessels and is required for embryonic vasculature by producing lysophosphatidic acid. *J. Biol. Chem.* **281**, 25822-25830.
Thisse, C. and Thisse, B. (2008). High-resolution in situ hybridization to whole-mount zebrafish embryos. *Nat. Protoc.* **3**, 59-69.
van Meeteren, L. A. and Moolenaar, W. H. (2007). Regulation and biological activities of the autotaxin-LPA axis. *Prog. Lipid Res.* **46**, 145-160.
van Meeteren, L. A., Ruurs, P., Stortelers, C., Bouwman, P., van Rooijen, M. A., Pradère, J. P., Pettit, T. R., Wakelam, M. J., Saulnier-Blache, J. S., Mummery, C. L. et al. (2006a). Autotaxin, a secreted lysophospholipase D, is essential for blood vessel formation during development. *Mol. Cell. Biol.* **26**, 5015-5022.
van Meeteren, L. A., Ruurs, P., Stortelers, C., Bouwman, P., van Rooijen, M. A., Pradère, J. P., Pettit, T. R., Wakelam, M. J. O., Saulnier-Blache, J. S., Mummery, C. L. et al. (2006b). Autotaxin, a secreted lysophospholipase D, is essential for blood vessel formation during development. *Mol. Cell. Biol.* **26**, 5015-5022.
Wang, G., Cadwallader, A. B., Jang, D. S., Tsang, M., Yost, H. J. and Amack, J. D. (2011). The Rho kinase Rock2b establishes anteroposterior asymmetry of the ciliated Kupffer's vesicle in zebrafish. *Development* **138**, 45-54.
Ye, X. Q., Hama, K., Contos, J. J. A., Anliker, B., Inoue, A., Skinner, M. K., Suzuki, H., Amano, T., Kennedy, G., Arai, H. et al. (2005). LPA3-mediated lysophosphatidic acid signalling in embryo implantation and spacing. *Nature* **435**, 104-108.
Yost, H. J. (1999). Diverse initiation in a conserved left-right pathway? *Curr. Opin. Genet. Dev.* **9**, 422-426.
Yuan, X. B., Jin, M., Xu, X. H., Song, Y. Q., Wu, C. P., Poo, M. M. and Duan, S. M. (2003). Signalling and crosstalk of Rho GTPases in mediating axon guidance. *Nat. Cell Biol.* **5**, 38-45.
Yukiura, H., Hama, K., Nakanaga, K., Tanaka, M., Asaoka, Y., Okudaira, S., Arima, N., Inoue, A., Hashimoto, T., Arai, H. et al. (2011). Autotaxin regulates vascular development via multiple lysophosphatidic acid (LPA) receptors in zebrafish. *J. Biol. Chem.* **286**, 43972-43983.
Zhang, M., Zhang, J., Lin, S.-C. and Meng, A. (2012). β-Catenin 1 and β-catenin 2 play similar and distinct roles in left-right asymmetric development of zebrafish embryos. *Development* **139**, 2009-2019.

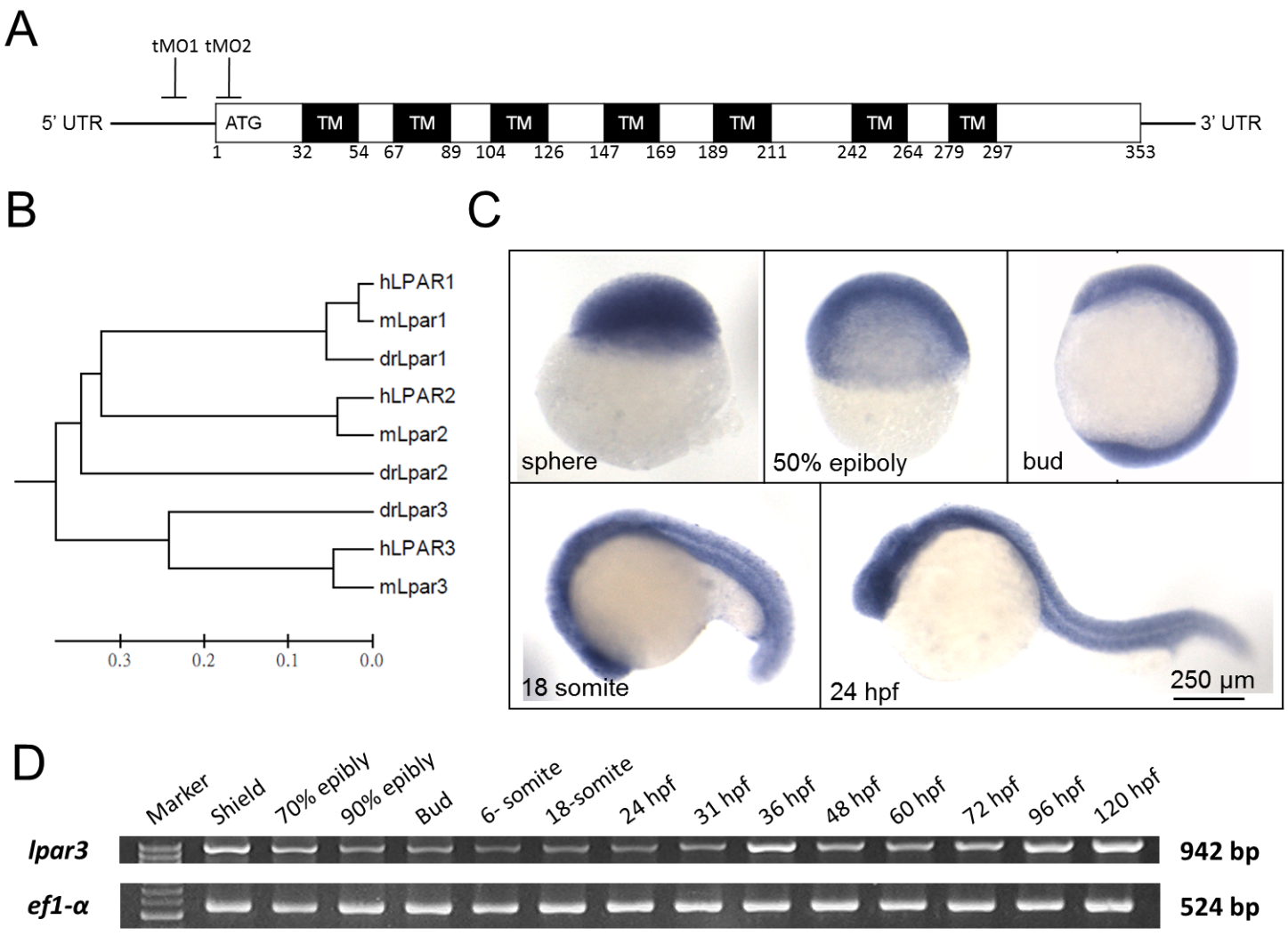

Fig. S1. Sequence analysis and expression profile of zebrafish *lpar3* gene. (**A**) Domain architecture of the G protein-coupled receptor Lpar3 in zebrafish. Lpar3 possesses evolutionarily conserved seven transmembrane domains (TMs) and translation-blocking MOs (tMO1 and tMO2) binding sites are indicated. Amino numbers flanking each transmembrane domain are shown. (**B**) Phylogenetic analysis of LPA receptors 1-3 from human (hLPAR1-3), mouse (mLpar1-3) and zebrafish (drLpar1-3). (**C**,**D**) WISH expression patterns (C) and RT-PCR analysis (D) of *lpar3* in zebrafish embryos at the designated stages. *ef1*-α was used as an internal control.

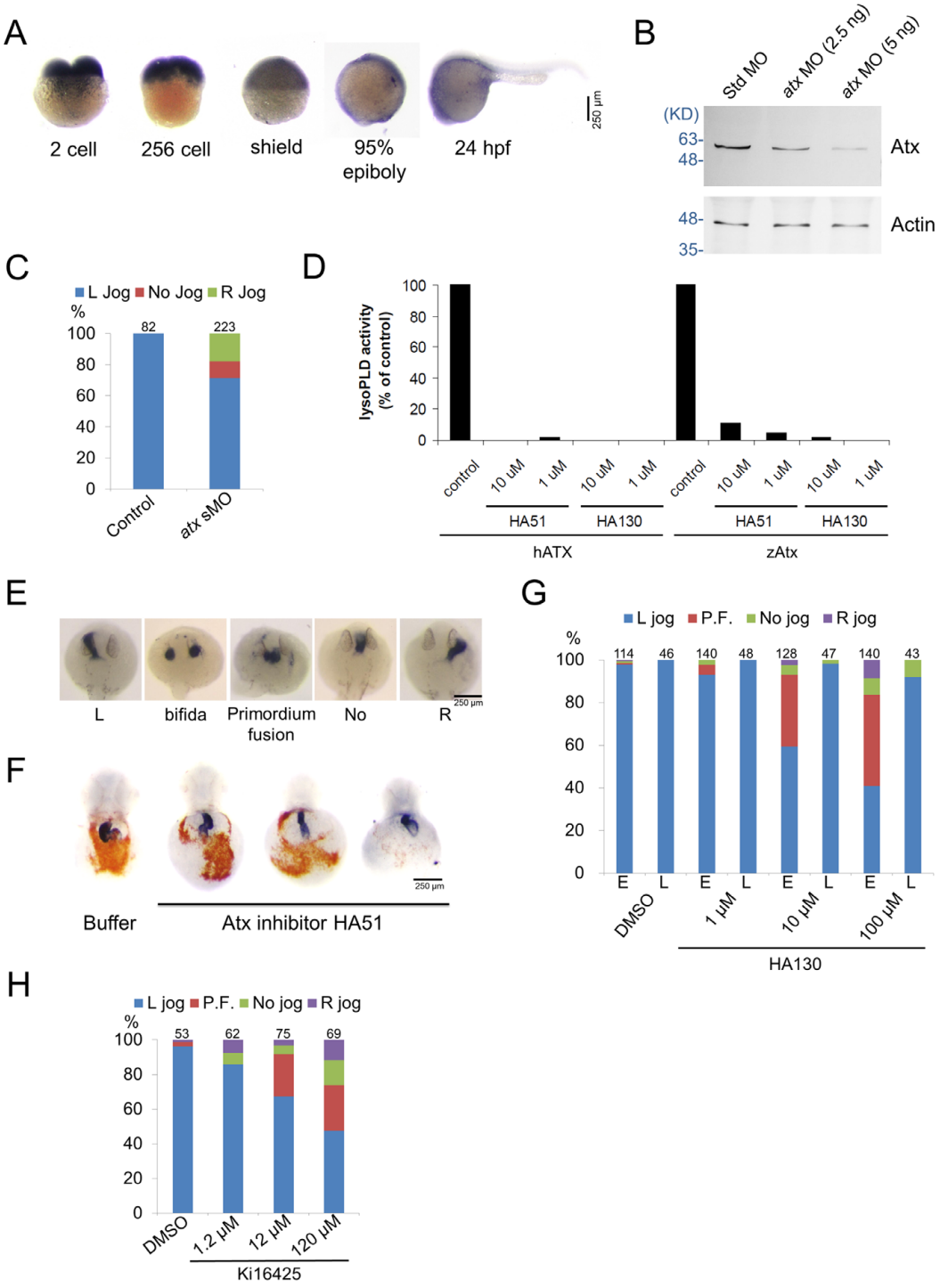

Fig. S2. Characterization of zebrafish Atx. (**A**) Expression patterns of zebrafish Atx during early development was observed by WISH. (**B**) Embryos injected with 5 ng Std MO, or 2.5 or 5 ng *atx* MO were cultured to shield stage and subjected to western blotting analysis. Expression of Atx was dose-dependently inhibited by *atx* MO. Molecular weight is shown in KD on the left-hand side. (**C**) Uninjected embryos and embryos injected with 2.5 ng of an *atx* splicing blocking MO (sMO) were incubated to 26-28 hfp and subjected to cardiac jogging analysis by WISH against *cmlc2*. Total number of embryos used in each treatment is shown on top of each column hereafter. (**D**) Human ATX (hATX) and zebrafish Atx (drATX) were expressed in HEK293T cells. LysoPLD activity of secreted Atx in the medium was measured by hydrolysis of FS3 (2.5 μM) as described in Materials and methods. (**E**) Representative patterns of cardiac jogging phenotypes in Atx-LPAR3 loss-of-function conditions. (**F**) Embryos were injected with or without HA51 at the one-cell stage, incubated and fixed at 48 hpf. Fixed embryos were subjected to o-dianosidine staining and WISH against *cmlc2*. Representative images are shown. (**G**) Cardiac jogging of embryos incubated with various concentrations of HA130 from 50% epiboly to tail bud stage (marked by 'E' for early) or embryos incubated with various concentrations of HA130 from 60% epiboly to tail bud stage (marked by 'L' for late) was examined and quantified (n=3). (**H**) Cardiac jogging of embryos incubated with various concentrations of Ki16425 from 50% epiboly to tail bud stage was examined and quantified (n=3).

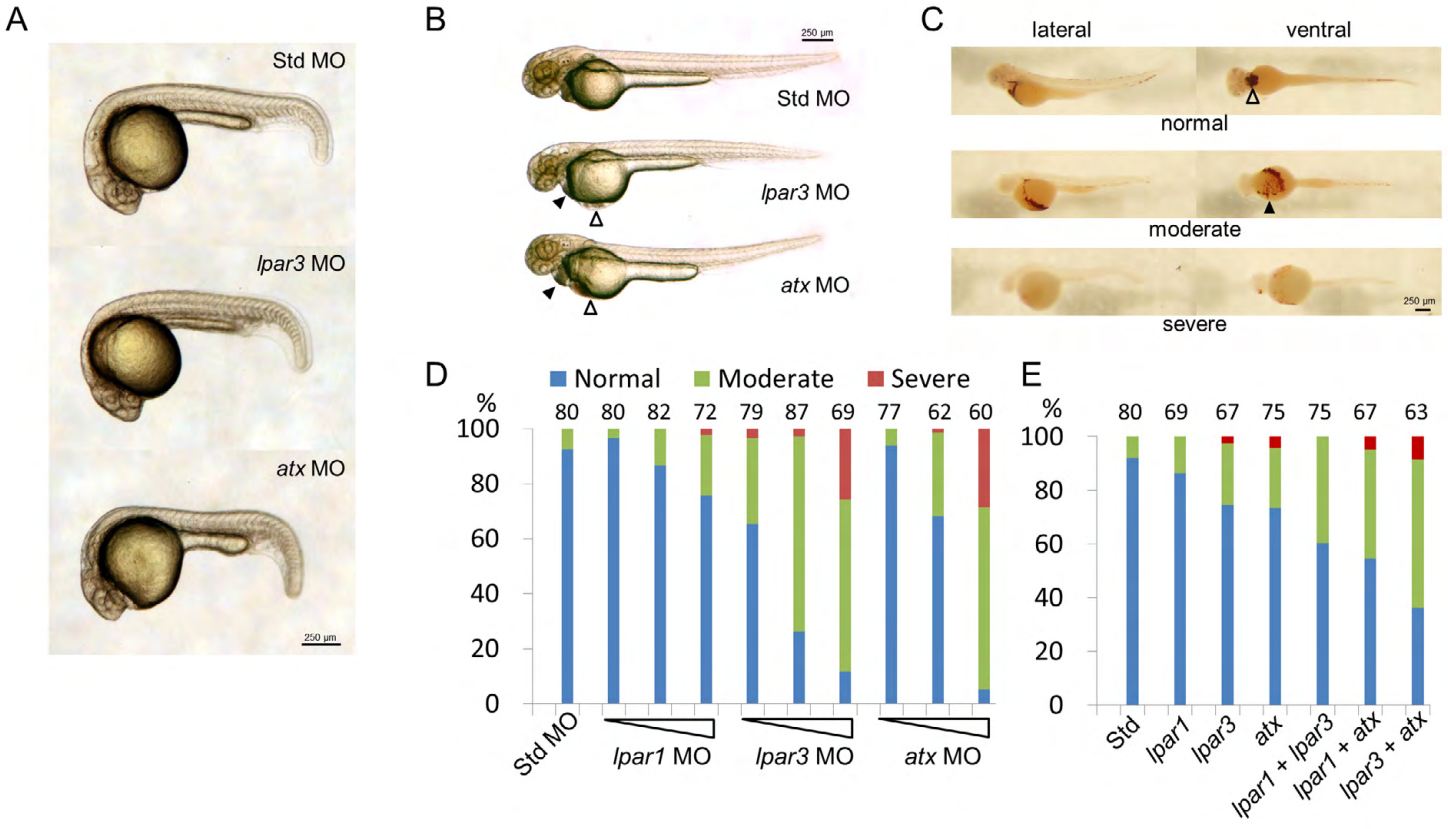

Fig. S3. Knockdown of *atx* and/or *lpar3* causes cardiac edema and blood pooling. (**A**,**B**) Embryos injected with *atx* or *lpar3* MOs were examined and photographed at 24 (A) and 48 (B) hpf. Cardiac edema (filled arrowheads) and blood pooling (open arrowheads) appeared at the ventral side of the yolk in both *atx* and *lpar3* morphants were observed (B). (**C**) Embryos injected with *atx* or *lpar3* MOs were fixed and stained with o-dianosidine to reveal erythrocytes (brown staining). The treated embryos were positioned and photographed from the lateral view or ventral view. In the normal condition (top row), erythrocytes concentrated in pericardiac cavity (open arrowhead) and major vessels; however, in moderate defective embryos (middle row), erythrocytes spread out to the ventral side of the yolk (filled arrowhead); in the most severe condition (lower row), were reduced erythrocytes and hemorrhage in brain and/or eyes were sometimes observed (ventral view). (**D**) Dose-dependent disturbance of erythrocyte distribution was found in embryos injected with 1.25, 2.5 and 5 ng per embryo of *lpar1*, *lpar3* or *atx* MOs. Std MO at 5 ng was used as a control (n=3). (**E**) Embryos were injected with single or different combinations of 1.25 ng of the indicated MOs.

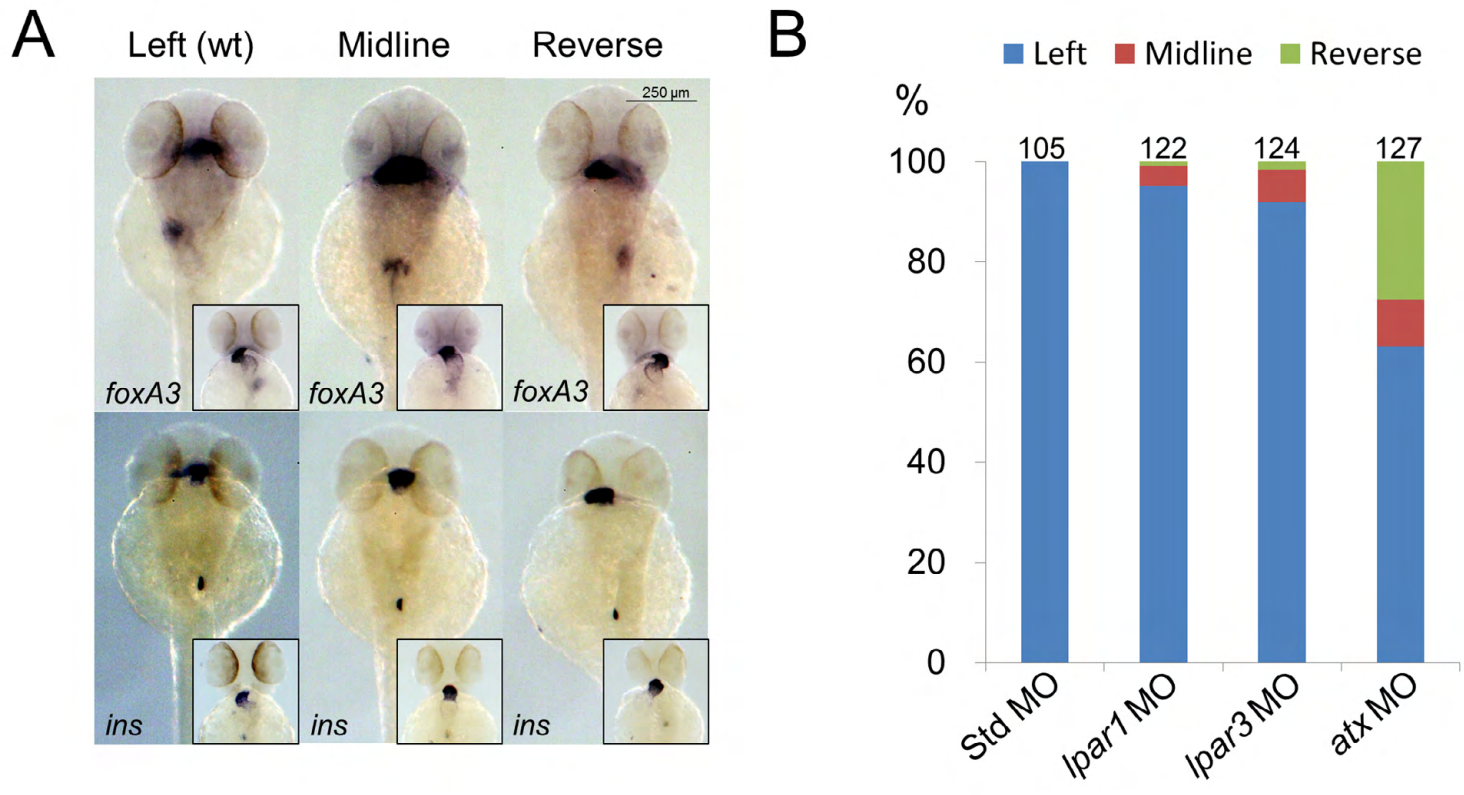

Fig. S4. Atx-Lpar3 axis mediates gut looping. Embryos injected with 5 ng Std MO, *lpar1* MO, *lpar3* MO or *atx* MO were incubated until 48 hpf, fixed and subjected to WISH against *foxA3*. (**A**) Three representative gut looping phenotypes, including L-loop gut liver bud (Left), defected midline gut (Midline) and reversed R-loop gut (Reverse), were shown by WISH against *foxA3* and *insulin* (*ins*). Insets showed corresponding cardiac looping patterns. (**B**) The percentages of each phenotype in all treatments are shown (n=3). Total number of embryos used in each treatment is shown on top of each column.

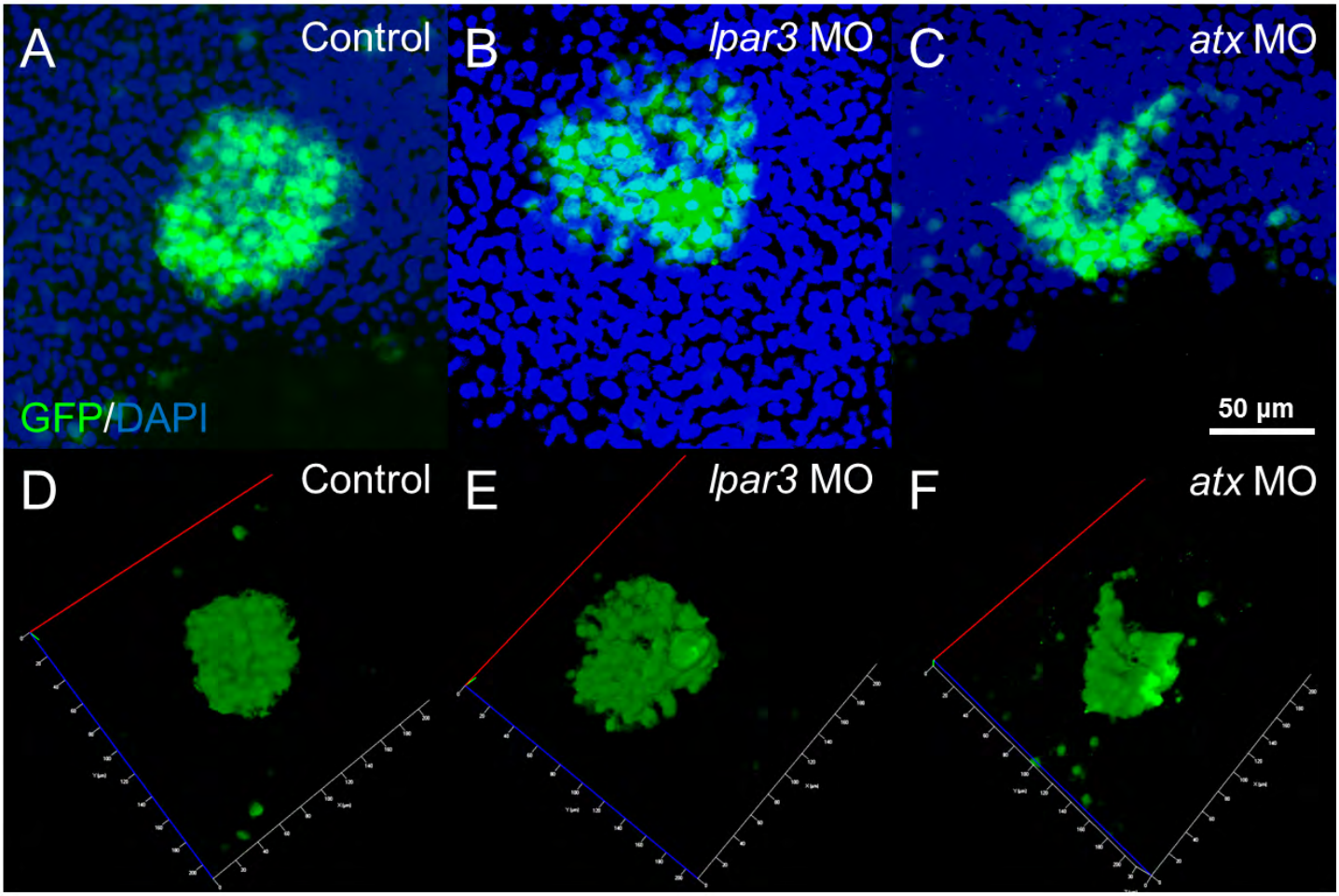

Fig. S5. KVs were deformed and dispersed in *lpar3* and *atx* morphants. (**A-F**) GFP and DAPI merged images (A-C) and GFP image 3D stack model (D-F) of KV in control embryo (A), and *lpar3* (B) and *atx* (C) morphants at the tail bud stage were examined and analyzed for cell dispersion and cell number under confocal microscopy. KV shown by GFP was from immunostaining of *sox17:GFP* embryos.

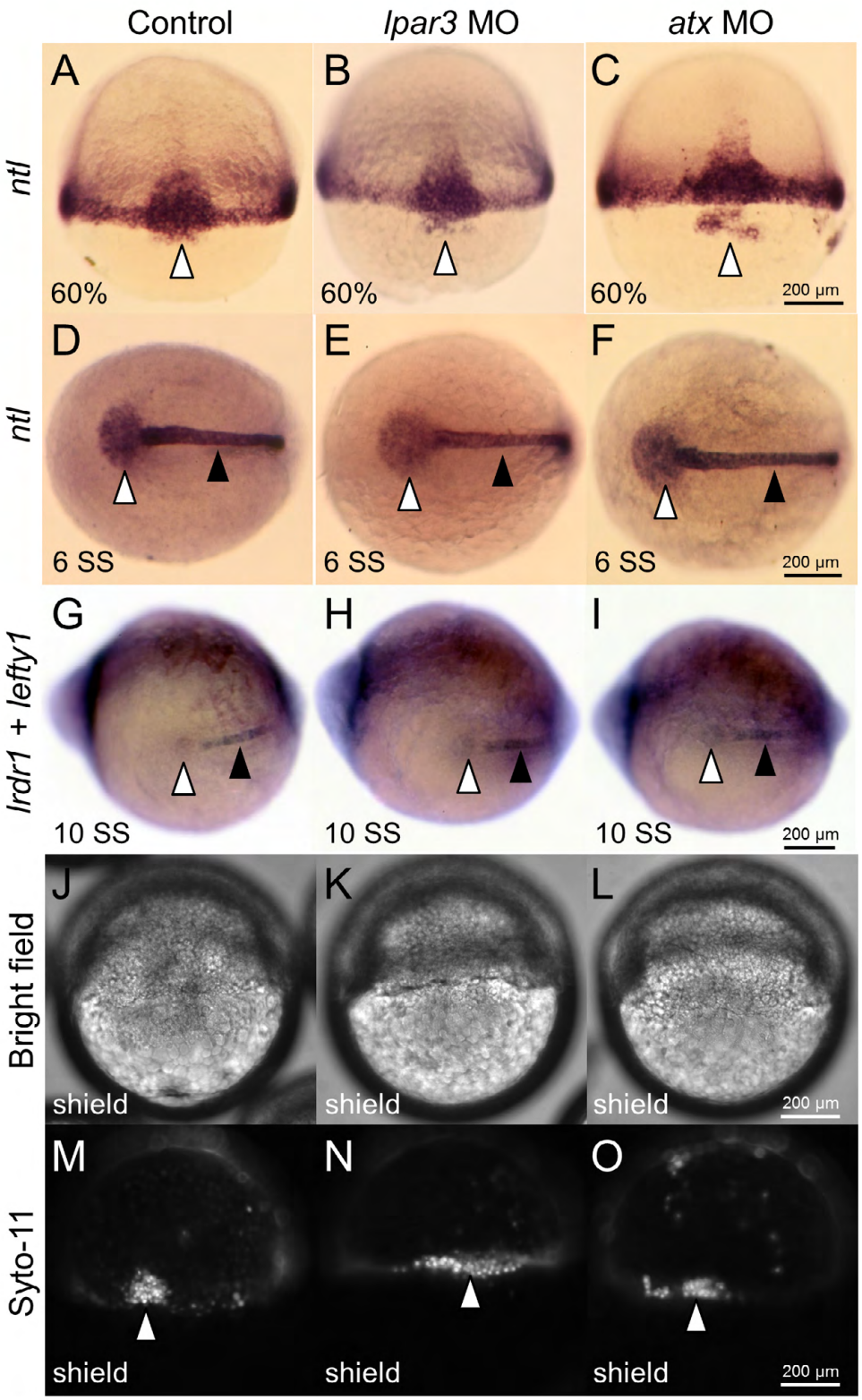

Fig. S6. DFC specification and cell number were not altered in *lpar3* and *atx* morphants. (**A-I**) Wild-type (Wt) embryos, *lpar3* and *atx* morphants were subjected to WISH against the DFC-specific marker *ntl* (A-F) at 60% epiboly and the six-somite stage (6 SS) and *lrdr1* + *lefty1* (G-I) at the ten-somite stage (10 SS; as indicated). Formation of DFCs and sustained expression of DFC-specific genes were observed in Wt embryos as well as in *lpar3* and *atx* morphants at the stages indicated (open arrowheads). Notochord expression of both *ntl* and *lefty1* were also observed (filled arrowheads). (**J-O**) Embryos were stained with vital dye SYTO-11 (10 µM) and examined at 6.5 hpf for DFCs endocytosis activity, cell clustering and cell number quantification. DFCs in *lpar3* (K,N) and *atx* (L,O) morphants formed as early as those in Wt embryos (J,M), with similar numbers, but are more dispersed as linear pattern and sometimes even separate into two groups.

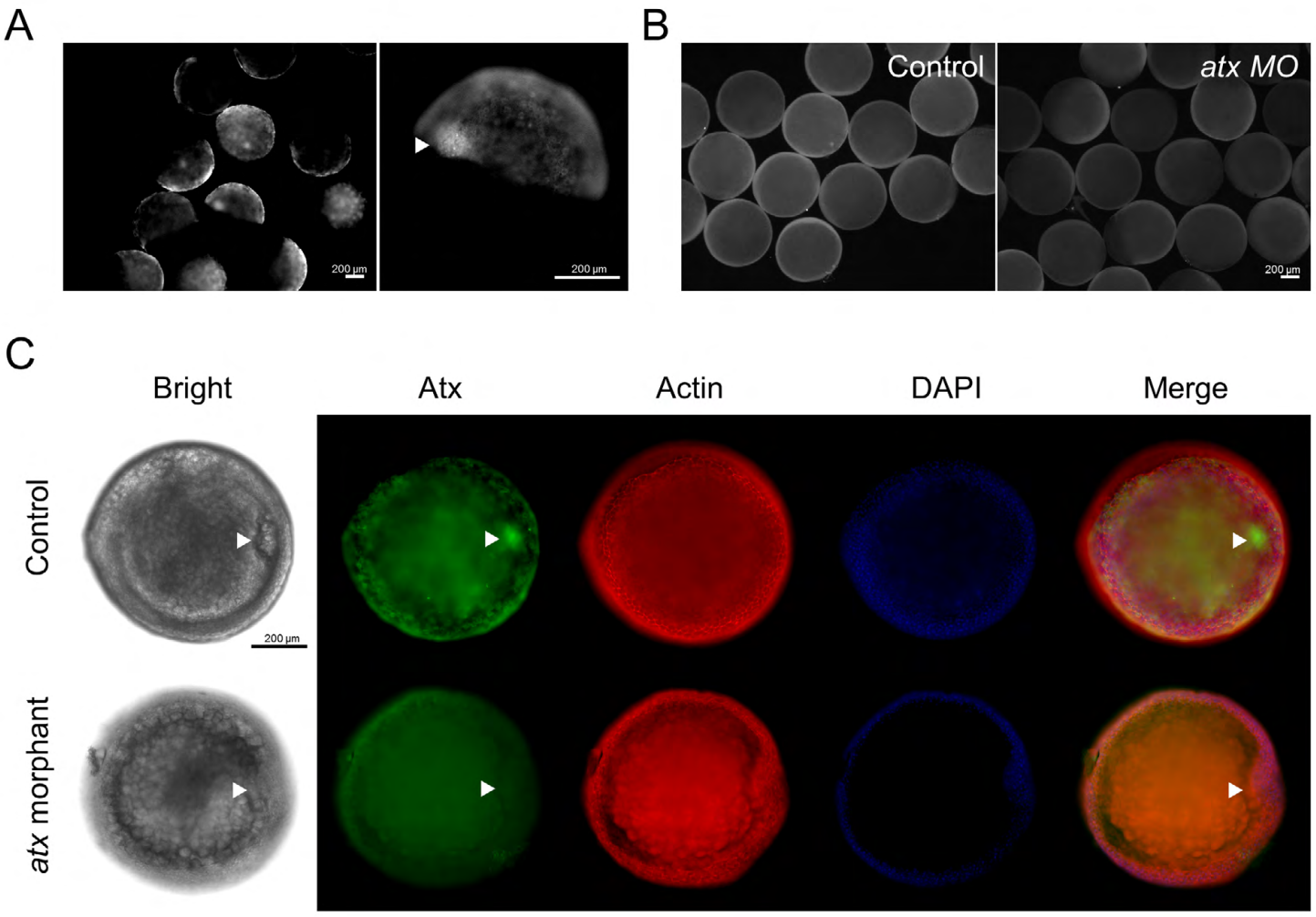

Fig. S7. Atx localizes in the shield during mid-epiboly stage. Atx was examined by immunofluorescence staining at the shield stage. (**A**) Atx was localized sporadically in blastomeres and concentrated in shield region (arrowheads) in control embryos. (**B**) The overall expression of Atx protein was notably reduced in *atx* morphants compared with that of control embryos. (**C**) When observed from the animal top view, Atx was found to be localized in shield blastomeres (arrowheads) in control embryos, but not those of *atx* morphants.

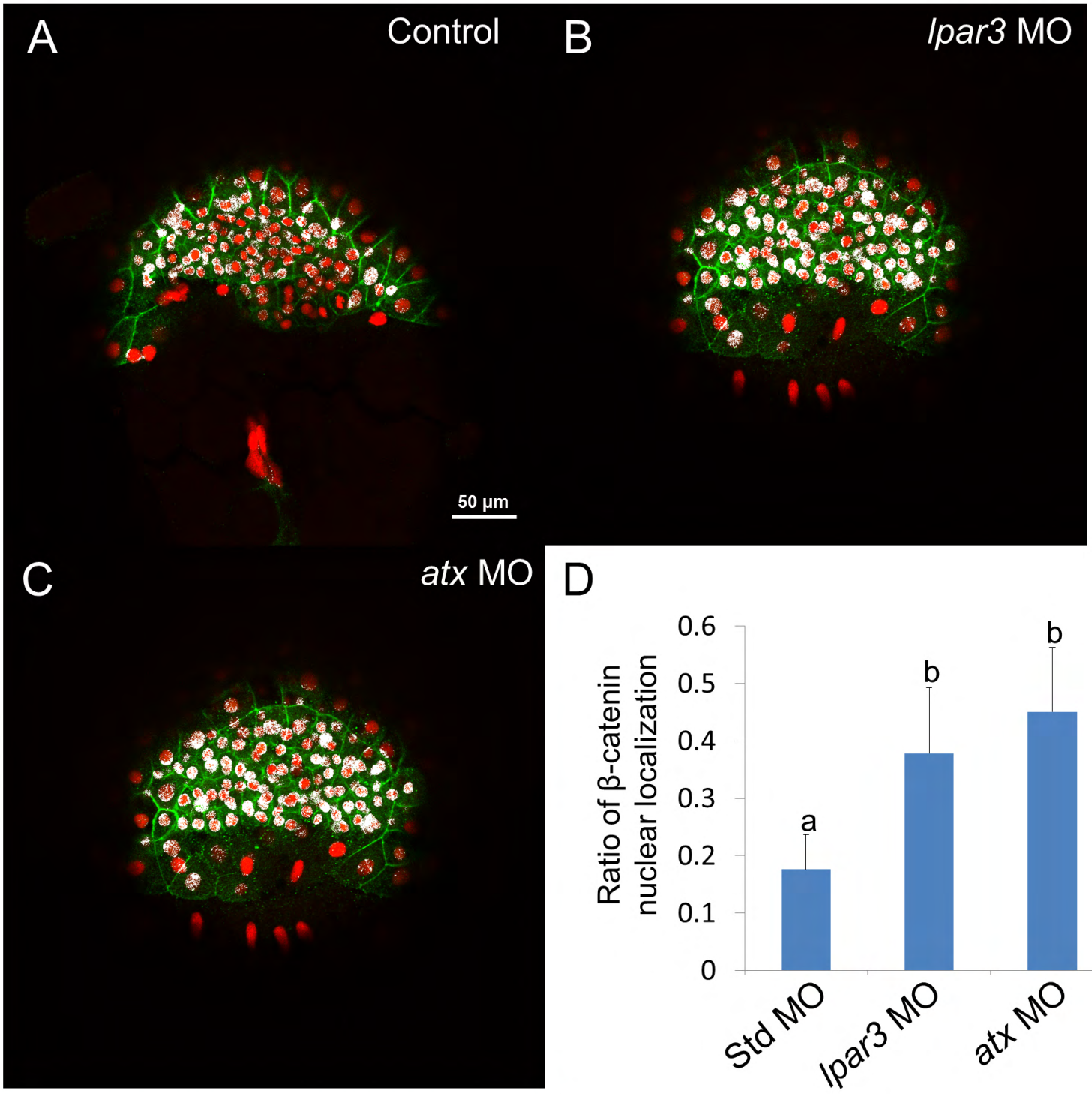

Fig. S8. Knockdown of Atx-Lpar3 signaling activates β-catenin. (**A-C**) Wild-type (Wt) embryos (A), and *lpar3* (B) and *atx* (C) morphants were fixed at the 60-70% epiboly stage and immunostained with anti-β-catenin (green) and DAPI (red). Forty-five stacks ranging from 8.3 to 12.45 µm below the surface was calculated for colocalization (as indicated by white signal) using ImageJ software, merged and shown. Nuclear β-catenin signal was stronger in *lpar3* and *atx* morphants than in Wt embryos. (**D**) Forty-five stacks in five embryos with respective treatments were quantified. groups denoted with different lettering refer to statistical significance ($P<0.05$).

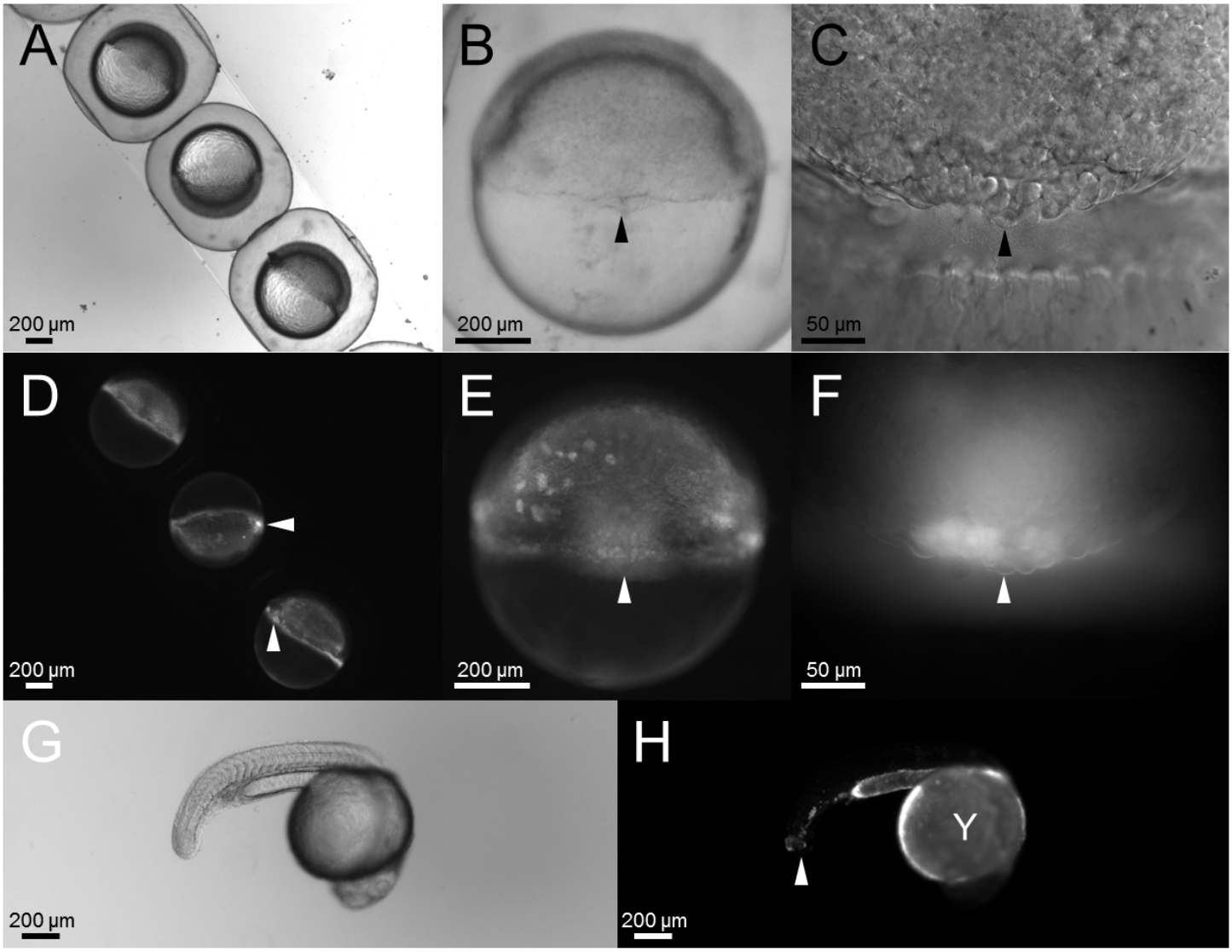

Fig. S9. DFC-targeted delivery of MOs. (**A-H**) Embryos at the 512-cell stage were injected with *lpar3* MO with a 3′ fluorescein modification into the YSL, cultured to mid-epiboly and examined at different magnifications under bright field (A-C) and dark field with a GFP cube (D-F). In addition to YSL, fluorescent MOs were enriched in DFCs (arrowheads in A-F), and also found in yolk (Y) and some tail cells at 24 hpf (arrowhead in H).